Finite Element Simulations of Biphasic Articular Cartilages With Localized Metal Implants

by

Krishnagoud Manda

December 2010
Technical Reports from
Royal Institute of Technology
Department of Mechanics
SE - 100 44 Stockholm, Sweden

Typsatt i $\mathcal{AMS}$-LaTeX

Akademisk avhandling som med tillstånd av Kungliga Tekniska högskolan i Stockholm framlägges till offentlig granskning för avläggande av teknologie licentiatexamen torsdagen den 16 december 2010 kl 10.15 i E3, Kungliga Tekniska högskolan, Osquars Backe 14, Stockholm.

Universitetsservice US–AB, Stockholm 2010

Finite Element Simulations of Biphasic Articular Cartilages With Localized Metal Implants

Krishnagoud Manda
Dept. of Mechanics, Royal Institute of Technology
SE-100 44 Stockholm, Sweden

Abstract

Articular cartilage is a specialized connective soft tissue that resides on the ends of long-bones, transfers the load smoothly between the bones in diarthrodial joints by providing almost frictionless, wear resistant sliding surfaces during joint articulation. Focal chondral or osteochondral defects in articular cartilage are common and show limited capacity for biological repair. Furthermore, changes in the bio-mechanical forces at the defect site may make the tissue more susceptible to continued degeneration. Alternatively, the contoured focal resurfacing metal implant can be used to treat such full thickness cartilage defects. Physiological and biomechanical studies on animal models with metal implant have shown good clinical outcomes. However, the mechanical behavior of cartilage surrounding the implant is not clearly known with respect to the joint function after treating such defects with metal implants and also to improve the implant design. We developed a simple 3-dimensional finite element model by approximating one of the condyles of the sheep knee joint. Parametric study was conducted in the simulations to verify different profiles for the implant, positioning of the implant with respect to cartilage surface, defect size and to show the mechanical sealing effect due to the wedge shape of the implant. We found the maximal deformations, contact pressures and stresses which constitute the mechanical behavior of cartilages. We also confirmed that using a metal implant to fill the full thickness chondral defects is more beneficial than to leave the defect untreated from mechanical point of view. The implant should be positioned slightly sunk into the cartilage based on the defect size, in order to avoid damage to the opposing surface. The larger the defect size, the closer the implant should be to the flush. We also simulated the time dependent behavior of the cartilages. In all the simulations, a static axial loading was considered. The wedge shape of the implant provided the mechanical sealing of the cartilage surrounding the implant. The determined deformations in the cartilages immediately surrounding the implant are instrumental in predicting the sticking-up of the implant into the joint cavity which may damage opposing soft tissues.

Descriptors: finite element analysis, articular cartilage defects, knee joint, metal implant, poroelastic, biphasic, ABAQUS

Preface

This work investigates the application of metal implants for treating small full thickness chondral defects in the knee joint. In the first part, a brief introduction, method development, short discussion of chosen results and a description of forces acting at the knee are presented. The second part of this thesis is a collection of the following two articles.

Paper 1. Manda K., Ryd L. and Eriksson A., 2010
"Finite element simulations of a focal knee resurfacing implant applied to localized cartilage defects in a sheep model", Submitted to Journal of Biomechanics.

Paper 2. Manda K. and Eriksson A., 2010
"Time dependent behavior of cartilages surrounding a metal implant for full thickness cartilage defects of various sizes: a finite element study", Submitted to Biomechanics and Modeling in Mechanobiology.

Division of work between authors
The research project was originally initiated by Prof. Anders Eriksson (AE) who also acted as the main supervisor and advisor of the this work. Leif Ryd (LR) has supplied ideas and formulated a set of questions which formed the basis for the work. Moreover, Krishnagoud Manda (KM) has continuously discussed the progress of the project throughout the course of the work with AE.

Paper 1
The modeling and simulations were performed by KM with feedback from AE. The paper was written by KM with input from AE and LR.

Paper 2
The modeling and simulations were performed by KM with feedback from AE. The paper was written by KM with input from AE.

Contents

Part I

Overview and summary

CHAPTER 1

Introduction

Mechanical modeling of the biological structures has been emerging, in recent years, as an important research field to address and solve clinical-relevant problems. Many researchers have been simulating the complex physiological behavior of the load carrying joints of a human body using numerical methods to estimate and understand the causes and remedies of the joint deterioration or degeneration due to mechanical loads arising from daily activities of life. Finite element modeling (FEM), which describes the physical behavior of the structure, is a well known numerical technique, has proven to be of incalculable benefit in the modeling of biomechanical systems by making appropriate simplifications. The simplifications that are appropriate for one research question may be totally inappropriate for another. Generally, FEM involves geometrical representations, material representations by constitutive laws and boundary conditions (Cook et al. 2002). Finite element modeling could be helpful to predict stresses/strains, in providing insight into mechanisms of injury, effects of treatment and to analyze the role of mechanical factors in degenerative conditions in the joint.

1.1. Knee anatomy

The knee is one of the largest and the most complex diarthrodial joints in the human body, controlling the relative motion between lower and upper parts of the leg, and is lubricated by synovial fluid. The structure of knee joint, enclosed in a joint capsule, consists of three primary bones (tibia, femur and patella), connected by stabilizing structures (ligaments) and forms the tibiofemoral and patellofemoral joints. There are four primary ligaments in the knee: anterior cruciate, posterior cruciate, medial collateral, and lateral collateral ligaments. There are thin layers of cartilage residing on the articulating surfaces associated with all the three bones, and menisci (of semi-circular shape) layered between the distal and proximal ends of the femoral and tibial cartilage layers, Fig. 1.1. The menisci are fixed within the knee joint by attachments to the proximal tibial surface.

1.2. Cartilage structure and behavior

Articular cartilage (AC) has a complex tissue structure and plays a vital role in the functioning of a musculoskeletal system by providing a long-lasting lubricious low friction gliding surface in the diarthrodial joints (Mow et al. 1993).

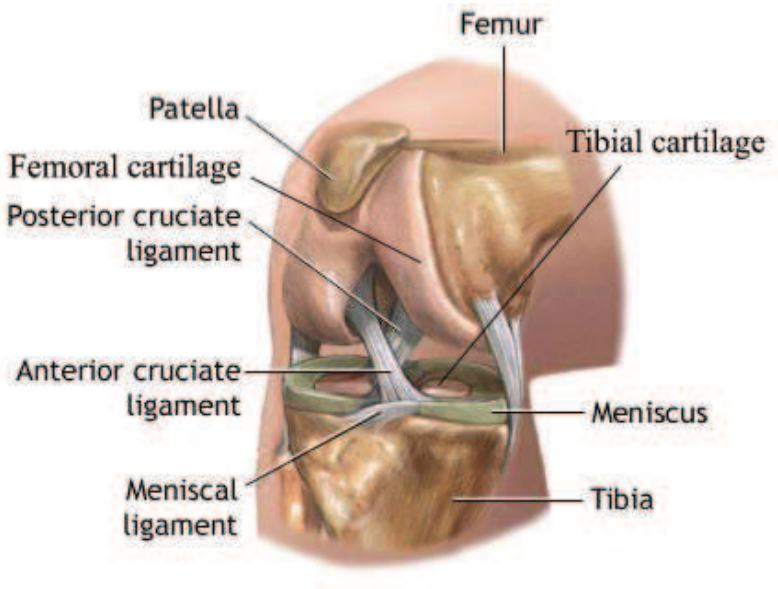

FIGURE 1.1. Anatomy of a human knee joint. Image reproduced from A.D.A.M., Inc.

However, the contact of just articular cartilage surfaces between the bones is localized due to the lack of congruity in the joint. The menisci (medial and lateral) maximize the congruency, and thus also the contact area between the two relatively incongruent surfaces in the joint. Thus, AC and menisci effectively redistribute the loads (Walker and Erkman 1975; Fukubayashi and Kurosawa 1980) over a larger contact area, thereby minimizing the contact stresses and dissipating parts of the mechanical energy so that the joint structure is protected from impact force. Normal cartilage exhibits remarkable lubricating and wear properties with a very low coefficient of friction, typically in the range of 0.001-0.03 (Mow et al 1980). In this section, the structure and mechanical properties of cartilage are briefly overviewed.

Articular cartilage is composed of a solid phase saturated with interstitial fluid (70-80% by wet weight) and mobile ions. The solid phase consists of cartilage cells (chondrocytes), sparsely distributed (1% to 10% by volume) within a fluid-filled extracellular matrix (ECM) which is composed mainly of collagens and proteoglycans (Bae and Sah 2008). The material properties of cartilage depend primarily on the properties of the ECM. These components are not uniformly distributed in the matrix. Instead, cartilage can be divided into four zones: superficial, middle, deep, and calcified (Mow et al. 2004). The superficial articular zone is the thinnest one and forms the gliding surface of the joint. This zone is characterized by high water content (85%), relatively low quantities of proteoglycan, flattened chondrocytes and high quantities of

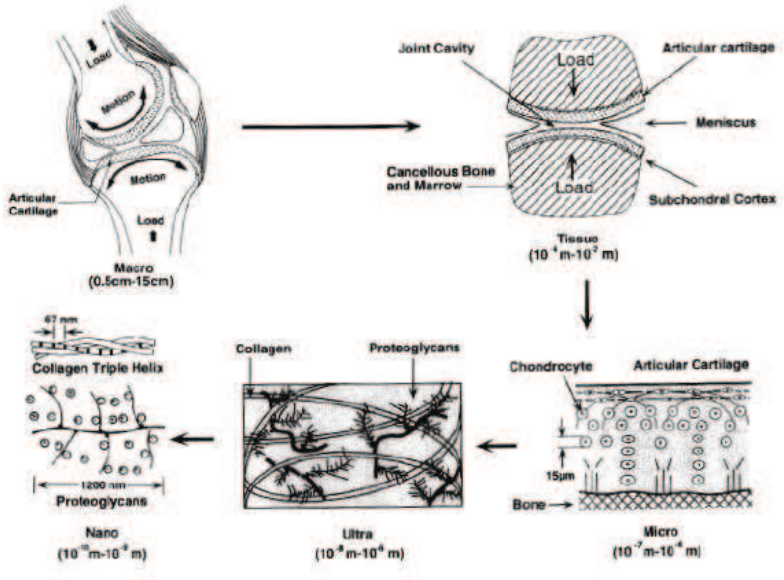

FIGURE 1.2. Hierarchical structure of diarthrodial joints and articular cartilage. Image reproduced from Mow et al. (2004)

collagen fibrils arranged parallel to the articular surface. The middle zone, in contrast, has round chondrocytes, the highest level of proteoglycan among the four zones, and a random arrangement of collagen. The deep zone is characterized by collagen fibers with largest diameters arranged perpendicular to the subchondral bone, columns of chondrocytes arrayed along the axis of fibril orientation and lower water content (approximately 60%). The calcified zone is partly mineralized, and is the transition layer between cartilage and underlying bone. From a biomechanical point of view, the highly organized collagen network and the charged proteoglycans network are the most important components in the articular cartilage (Mow et al. 2004; Bae and Sah 2008). The relation between cartilage structure and its mechanical behavior can be briefly explained as follows.

1.2.1. *Viscoelastic behavior*

The important mechanisms that contribute to the viscoelastic behavior of cartilages (Mow et al 1980; Suh and Bai 1998; Mow et al. 2004; Mow and Hung 2001; Wilson et al. 2005b) are the frictional drag force of interstitial fluid flow through the porous solid phase (i.e. the flow-dependent mechanism), and the time-dependent deformability of the solid matrix (i.e., the flow-independent mechanism). When the cartilage is loaded, fluid flows out of the solid matrix, which reduces the volume of the whole cartilage. At equilibrium, no fluid flow or fluid pressure gradients exist, and the entire load is carried by the solid

matrix. Upon removal of load or deformation, cartilage recovers its initial configuration, due to the elasticity of the solid phase and the increased osmotic pressure within the tissue. Fluid movement in a loaded cartilage is governed by the hydraulic permeability (k) of the solid phase. The permeability is also highly dependent on pore sizes in the extracellular matrix. When the tissue is deformed, pore sizes change, making the permeability strain dependent.

1.2.2. *Compressive behavior*

Cartilage exhibits large depth-associated variations, both in compression and tension. The compressive modulus, a measure of intrinsic compressive stiffness, is low in the superficial layer and increases with depth from the articular surface (Mow and Hung 2001; Bae and Sah 2008). The proteoglycans are mainly responsible for the variation in biomechanical characteristics of cartilage in compression. When the cartilage is loaded in compression, volumetric changes occur because of fluid movement within the tissue. With these volumetric changes the fixed charge density inside the tissue increases, and thereby also the internal osmotic-pressure and chemical-expansion stress. Hence, the effective stiffness of the tissue increases with decreasing volume (Wilson et al. 2005b).

1.2.3. *Tensile behavior*

The tensile stiffness, in contrast to compression, decreases with depth and as the axis of extension deviates from the split-line direction. The tensile modulus of cartilage depends on the collagen fibril density, fibril orientation and the amount of collagen cross-linking (Bae and Sah 2008). When cartilage is tested in tension the collagen fibrils and proteoglycan molecules are aligned and stretched along the axis of loading. For small deformations, when the tensile stress in the specimen is relatively small, a nonlinear toe-region is seen in the stress-strain curve, due to realignment of the collagen fibrils, rather than stretching of these fibers. For larger deformations, and after realignment, the collagen fibrils are stretched and therefore generate a larger tensile stress due to the intrinsic stiffness of the collagen fibrils themselves. Due to this phenomenon the tensile stiffness of cartilage is highly strain dependent (Akizuki et al. 1986; Mow and Hung 2001; Wilson et al. 2005b).

1.3. Cartilage defects and resurfacing implants

Damage or degeneration in the articular cartilage is a major problem that affects millions of people in the world. In 50% of the patients undergoing arthroscopy, articular cartilage defects are detected. The location of these lesions are predominantly on the medial femoral condyle (Curl et al. 1997). An important cause of lesions or defects is trauma in addition to osteoarthritis. Cartilage defects have been classified into the following groups (Brittberg et al 2000).

- grade 0: normal cartilage
- grade I: cartilage with softening and swelling

- grade II: partial-thickness defects with fibrillation or fissures on the surface that do not reach subchondral bone
- grade III: fissuring to the level of subchondral bone
- grade IV: exposed subchondral bone (full thickness defects)

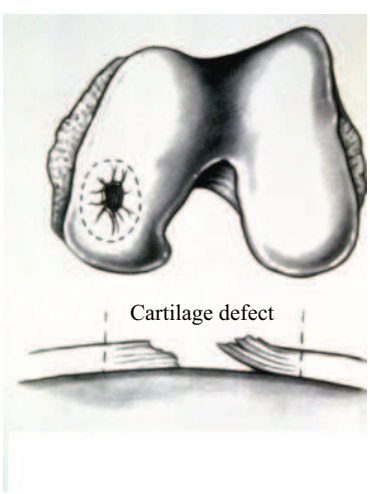

(a)

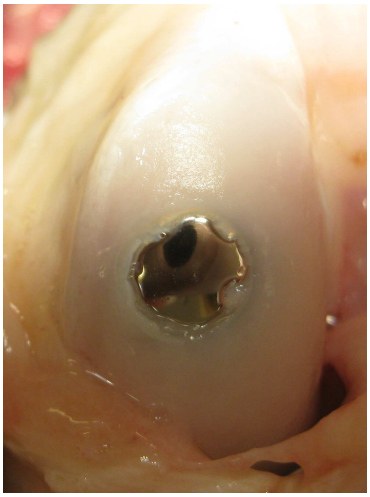

(b)

FIGURE 1.3. (a) Localized cartilage defect on femoral condyle. Reproduced from www.arthroscopy.com, (b) An example of knee condyle implanted with metal spherical profiled implant (Episurf Medical AB, Stockholm)

Recent studies have shown that focal articular surface defects (chondral or osteochondral) in the human knee may progress to degenerative arthritis. Such a defect is shown in Fig. 1.3(a). The changes in the biomechanical forces at a site of damage in the cartilage may make the tissue more susceptible to continued long-term degeneration. Various biological treatments are currently available which are mainly proposed for younger, active patients. These techniques are not so effective in older people. But, many middle aged patients are affected by localized cartilage defects and are fit for neither biological treatments nor traditional total joint replacement. Moreover, clinically, biological regeneration of cartilage becomes histologically different from the intact cartilage, with reduced mechanical quality compared to native tissue (Temenoff and Mikos 2000). Alternatively, a contoured articular prosthetic femoral resurfacing device (implant) is developed to offer a treatment to such full thickness chondral defects (Episurf Medical AB, Stockholm, HemiCAP^{TM} (2002)). The main goal of using metal plugs/implants, to fill the degenerated portion of the cartilage, is to seal the surrounding cartilage so that further damage can be prevented, and to re-establish the integrity of the joint articulating surface. Many researchers

have studied the safety, feasibility and reliability of the metal implants in animal models from a biological point of view. The first group who studied the metal implant filling cartilage defects is Custers et al (2007a,b, 2009a) using a rabbit model. But, they observed a considerable cartilage degeneration of the opposing articulating cartilage of the tibia. This may have been due to the sensitivity of such a small animal model (the healthy rabbit knee cartilage thickness is 0.3 mm) to small deviations in surgery procedures. Since then, many other experimental studies are reported on sheep or goat models (cartilage thickness is 0.7-1.5 mm). These studies are due to the suitability of an experimental sheep model for conducting in vivo orthopedic studies (Martini et al. 2001; Zarrinkalam et al. 2009). They showed promising results.

More recently, Episurf Medical AB, Stockholm have developed the metal resurfacing implants to treat the full thickness cartilage defects. They have been testing these implants on the sheep models, Fig. 1.3(b). Results are not yet fully documented, but are promising, and human testing is being planned.

Till date, the mechanical behavior of cartilages surrounding the implant has not been studied, even in the animal models. So it is important to understand the mechanical effect of the implant on the surrounding soft tissues, so that the implant design can be improved. Moreover, it is essential to understand the time dependent behavior of the cartilages as time plays an important role due to biphasic nature of cartilage. Any protrusion of metal implant into the joint cavity damages the opposing soft tissue (Becher et al 2008). In order to avoid this, the positioning of implant together with the behavior of the cartilages immediately surrounding the implant have to be studied. The experimental determination of stresses and deformations in the cartilages due to metal implant is technically challenging, time consuming and expensive. Hence, there is a need of developing a simple model to simulate the in vivo behavior of cartilages with the implant and to study parametrically the effect of its positioning for different defect sizes. The numerical modeling of the joint would facilitate us to understand the in vivo behavior of the joint with the localized metal implants.

1.4. Knee joint loads

The knowledge of the loads acting on the joints during daily activities of life is essential to simulate the physiological environment using numerical methods. The loads acting at the human knee are very complex in nature. Many researchers have worked on either measuring loads using experimental techniques or deriving loads by mathematical modeling at the knee joint. A detailed description of loads at the knee joint is reviewed from the literature in chapter 5. The moments and forces about a knee vary substantially for different daily activities. The most dangerous critical load in the knee joint is axial load (1 to 8 times body weight) that transfers between the bones through cartilages during the daily activities. The cartilages are subjected to heavy compression

and high pressures due to this load. Song et al (2008) observed a accumulation of strain in the intact cartilages in a sheep model due to repeated cyclic load simulating normat gait. This maximum cumulative nominal strain was increased to 55% after one hour. The effect of cyclic loading can be roughly simulated by a high magnitude constant static load on the joint. Hence, in this work a static axial load of 2 BW (ramped up during 1 s, and then held constant) is considered to simulate the cartilage behavior in the joint with a metal implant.

1.5. Objectives

The modeling of biphasic soft tissues for predicting their physiological behavior is a challenging task for an engineer. In this study, an attempt has been made to model biphasic articular cartilage as porous saturated medium. The main objective of this study was to develop a numerical finite element model to investigate the mechanical feasibility of the metal implant to treat full thickness cartilage defects. Subsequently, we wanted to determine the in vivo behavior of the cartilages surrounding the metal implant. The shape of the articulating surface and positioning of the implant were studied for various defect sizes. The effect of implant wedge shape on the mechanical sealing of the implant was studied. Time plays an important role in the tissue behavior. Hence, a fairly long time scale was considered in the simulations. The effect of time on the cartilage behavior in the joint was then studied.

1.6. Outline of thesis

The thesis is composed of two parts. The geometrical representation and modeling aspects used in this work are described in Chapter 2, along with the modeling of biphasic cartilage as a saturated porous medium (poro-elastic) using finite elements. In chapter 3, the data obtained from finite element modeling and their physiological relevance are discussed. Chapter 4 deals with the summary of two articles. The in vivo forces acting at the knee and their measurement techniques are briefly discussed in chapter 5. Lastly, the main conclusions and future scope are found in chapter 6. The second part of the thesis consists of the resulting papers.

CHAPTER 2

Methods

In this chapter, the constitutive models for representing articular cartilage ('AC') are briefly described. Later, the model development for a sheep knee and its finite element modeling by considering axial loading situation are presented together with the poro-elastic model in the commercial FE software ABAQUS.

2.1. Constitutive models for articular cartilage

The biomechanical characterization of an articular cartilage is one of the most intensely studied topics in orthopaedic research. Historically, it is accepted that a biphasic model is well suited to characterize the physiological behavior of articular cartilage. In the literature, many material models for cartilage can be found, ranging from simple ones including the biphasic nature of cartilage to models that include all major individual components of the cartilage. The different constitutive models, and the evolution of the biphasic theory for modeling articular cartilage, are briefly discussed in this section.

2.1.1. *Preliminary models*

As discussed in section (1.2), articular cartilage is composed of water (70-80%) and a saturated solid phase with proteoglycans, collagen and other organic molecules. The fluid permeability of the cartilage is very low (in the order of $10^{-15}\mathrm{m}^4/\mathrm{Ns}$, Mow et al (1980)); it is quite difficult to squeeze the water out. Consequently, for short static or cyclic loading periods, the cartilage behaves mechanically as a single-phase solid material. Ateshian et al. (2007) established the equivalence between short time biphasic cartilage response and incompressible elastic material responses. Under these conditions, the simplest constitutive cartilage models are either single phase linear isotropic elastic incompressible, a nearly incompressible solid, or a viscoelastic solid (Hayes et al. 1972; Kempson et al. 1971). The incompressibility of the cartilage at short loading times is related to its high water content. These are the first attempts of biomechanical characterization of cartilage with elastic materials.

2.1.2. *Evolution of the biphasic model*

As the single-phase material models cannot capture interstitial fluid movement in articular cartilage, the first biphasic model accounting for fluid and solid phases as distinct components of the system was from the pioneering work by

Mow et al (1980). In this simple version, the solid phase is assumed to be isotropic linear, elastic, incompressible or nearly incompressible and the interstitial fluid to be incompressible and inviscous. This means that cartilage as a whole can only be compressed if fluid is exuded from the cartilage. The permeability of cartilage is assumed to be a constant in the linear biphasic theory. But, the flow-limiting effects at higher strains, where the permeability of the tissue was found to decrease exponentially with the increasing strain, was observed by Mansour and Mow (1976). This effect was then incorporated into the biphasic theory by introducing the exponential strain dependent permeability (Lai and Mow 1980), resulting in a non-linear biphasic model. This non-linear model predicts a more realistic physiological behavior of the cartilage. Over the next couple of decades, the biphasic theory was validated by many researchers for various situations. Some important mathematical models from the literature (Wilson et al. 2005b) are discussed in the sequel.

2.1.3. *Basic equations of biphasic model*

In the biphasic theory, articular cartilage is composed of a mixture of extracellular matrix as the porous solid phase (20 % of the total tissue mass by weight) and interstitial fluid as the fluid phase (80 %) (Mow et al 1980). The biphasic equations by Mow et al (1980) are based on the assumptions that: the biphasic mixture is chemically inert and immiscible; each phase is intrinsically incompressible; the solid phase is linear elastic; the strains are infinitesimal; the fluid phase is inviscid; and the inertia forces are negligible. Denoting the whole volume of mixture as V, the volume fraction of each phase is given by

$$n_i = dV_i/dV \qquad i = s, f \tag{2.1}$$

with subscripts s and f are for solid and fluid phases, respectively. The saturation condition in the cartilage holds as

$$n_s + n_f = 1 \tag{2.2}$$

The total stress acting at a point in the tissue is given by the sum of the solid and fluid stresses,

$$\sigma_{tot} = \sigma_E - pI, \tag{2.3}$$

where σ_E is the effective stress tensor due to elastic deformation of the solid phase, p is the hydrostatic fluid pressure from the fluid phase and I is the unit tensor. For linear isotropic elasticity the effective stress tensor is given by

$$\sigma_E = \lambda e_s I + 2\mu\epsilon \tag{2.4}$$

where e_s is the cubic dilatation, ϵ is the strain tensor, and λ and μ are the first and second Lamé constants, respectively. These Lamé constants and the aggregate modulus of the solid matrix H_A, used in the biphasic model (Mow et al 1980) are related to Young's modulus and the Poisson ratio, E and ν, as

$$H_A = \lambda + 2\mu, \qquad E = \frac{\mu(3\lambda + 2\mu)}{\lambda + \mu}, \qquad \nu = \frac{\lambda}{2(\lambda + \mu)} \tag{2.5}$$

In the absence of mass exchange, the total mass change must be equal to the amount of fluid flow through the surface of the tissue. By assuming that each phase is incompressible and that the material is fully saturated, the continuity equation (law of conservation of mass) for the mixture is given by

$$\nabla \cdot (n_s \overrightarrow{v_s} + n_f \overrightarrow{v_f}) = 0 \tag{2.6}$$

or

$$\nabla \cdot \overrightarrow{v_s} + \nabla \cdot (n_f(\overrightarrow{v_f} - \overrightarrow{v_s})) = 0 \tag{2.7}$$

where $\overrightarrow{v_f}$ and $\overrightarrow{v_s}$ are the velocities of the fluid and solid phases, respectively. The vector $n_f(\overrightarrow{v_f} - \overrightarrow{v_s})$ gives the relative velocity of the fluid phase with respect to the solid phase, i.e., the fluid flow through the surface of the mixture. According to Darcy's law the fluid flux is related to the hydrostatic fluid pressure, as

$$n_f(\overrightarrow{v_f} - \overrightarrow{v_s}) = -k\nabla p \tag{2.8}$$

where k is the hydraulic permeability. With Eq. (2.8) the law of conservation of mass, Eq. (2.7), becomes

$$\nabla \cdot \overrightarrow{v_s} + \nabla \cdot (k\nabla p) = 0 \tag{2.9}$$

The depth dependency of articular cartilage (section 1.2) can be included by a depth dependent stiffness or permeability (Wang et al. 2001; Chen et al. 2001). The isotropic biphasic model has been used to analyze confined, unconfined compressions (Ateshian et al. 1997) for normal and osteoarthritic cartilage.

The fluid flow-dependent visco-elasticity can be included in the linear biphasic model, but it does not include features like exponential strain-dependent permeability, anisotropy caused by the collagen network, flow-independent viscoelasticity and the swelling behavior of cartilage (Wilson et al. 2005b).

2.1.4. *Strain-dependent permeability*

As discussed before, the permeability of cartilage is strain dependent. According to Lai et al. (1981), the strain-dependent permeability can be described as

$$k = k_0 \exp(M e_s) \tag{2.10}$$

where k_0 and M are material constants and e_s is the dilatation of the solid matrix. In terms of void ratio ($e = n_f/n_s$) this can be written as (van der Voet 1997),

$$k = k_0 \left(\frac{1+e}{1+e_0} \right)^M \tag{2.11}$$

where e and e_0 are current and initial void ratios, respectively.

Articular cartilage is a complex material, being both inhomogeneous and highly anisotropic due to its complex collagen network. In the literature, several models can be found which include these features. The most important and widely used models are presented in the following sections.

2.1.5. *Transversely isotropic models*

A special subclass of orthotropy is transverse isotropy, which is characterized by a plane of isotropy at every point in the material. In a transversely isotropic cartilage, all fibrils are assumed to run in the same direction. Longitudanal direction is parallel to the fibrils, and the transversal directions are perpendicular to the fibrils. Assuming the 1-2 plane to be the plane of isotropy at every point (fibrils lie in third direction $E_3 = E_L$), transverse isotropy requires that $E_1 = E_2 = E_T$, $\nu_{31} = \nu_{32} = \nu_{TL}$, $\nu_{13} = \nu_{23} = \nu_{LT}$ and $G_{13} = G_{23} = G_T$. The stresses in the solid are given by (Wilson et al 2003; Donzelli et al. 1999; Wilson et al. 2005b)

$$\begin{bmatrix}\sigma_{11}\\ \sigma_{22}\\ \sigma_{33}\\ \sigma_{12}\\ \sigma_{13}\\ \sigma_{23}\end{bmatrix} = \begin{bmatrix} 1/E_T & -\nu_{TT}/E_T & -\nu_{LT}/E_L & 0 & 0 & 0\\ -\nu_{TT}/E_T & 1/E_T & -\nu_{LT}/E_L & 0 & 0 & 0\\ -\nu_{TL}/E_T & -\nu_{TL}/E_T & 1/E_L & 0 & 0 & 0\\ 0 & 0 & 0 & 1/G_L & 0 & 0\\ 0 & 0 & 0 & 0 & 1/G_T & 0\\ 0 & 0 & 0 & 0 & 0 & 1/G_T \end{bmatrix}^{-1} \begin{bmatrix}\epsilon_{11}\\ \epsilon_{22}\\ \epsilon_{33}\\ \gamma_{12}\\ \gamma_{13}\\ \gamma_{23}\end{bmatrix} \tag{2.12}$$

where E, G and ν are Young's modulus, shear modulus and Poisson ratio, respectively. The notations L and T stand for longitudinal (along the fibrils) and transverse directions (perpendicular to fibrils), respectively. The transverse shear modulus G_T is given by

$$G_T = \frac{E_T}{2(1+\nu_{TT})} \tag{2.13}$$

Because of symmetry, there will be only five independent parameters, E_L, E_T, ν_{LT}, ν_{TT} and G_L, required for defining the model, as the relation must hold

$$\frac{\nu_{LT}}{E_L} = \frac{\nu_{TL}}{E_T} \tag{2.14}$$

2.1.6. *Fibril-reinforced models*

A significant description of the following fibril-reinforced and poro-viscoelastic models has been based on a review article by Wilson et al. (2005b).

The compression-tension non-linearity of the solid matrix can be included using a fibril-reinforced model (Soulhat et al. 1999; Li et al. 2000; Wilson et al. 2004, 2005b). In a fibril-reinforced model the fibril network (collagen network) contributes to the mechanical stiffness of the material, in addition to the isotropic matrix. The solid stress of a fibril-reinforced material is given by the sum of the matrix and fibril stresses. In the fibril-reinforced models for cartilage available in literature, fibrils are represented by springs between the nodes of the elements. Hence, the fibrils can only be represented in the direction of the elements. The solid stress of a fibril-reinforced material is given by the sum of the matrix and fibril stresses (Soulhat et al. 1999), as

$$\sigma_{E,i} = \sigma_{m,i} + \sigma_{f,i} \tag{2.15}$$

where $\sigma_{m,i}$ and $\sigma_{f,i}$ represent the normal stresses in direction i, in the nonfibrillar matrix and the collagen fibrils, respectively. In their earlier models the

stiffness of the collagen fibrils is represented by a linear spring with stiffness E_0, parallel to a nonlinear spring with stiffness $E_1 = E_\epsilon \epsilon_f$, where ϵ_f is the strain in the fibril direction. The fibril stress σ_f in these models is then given by

$$\begin{array}{ll} \sigma_f = (E_0 + E_\epsilon \epsilon_f)\epsilon_f & \text{for} \quad \epsilon_f \geq 0 \\ \sigma_f = 0 & \text{for} \quad \epsilon_f < 0 \end{array} \tag{2.16}$$

In the continuum fibril reinforced models, the fibril orientation is independent of the mesh. Hence, the fibrils can run in any direction, which enables the representation of a geometrically realistic collagen network. The fibrils are also modeled as viscoelastic materials (Wilson et al. 2005a,b).

The significant difference between the spring-based fibril-reinforced and the transversely isotropic model is that the fibrils in the fibril reinforced model resist only tension, while the transversely isotropic model has the same stiffness in compression and tension. Fibril reinforced biphasic models have been applied in unconfined compression, mainly for the characterization of the role of the collagen network in cartilage time-dependent response.

2.1.7. *Poro-viscoelastic models*

The time-dependent behavior of cartilage is caused by both fluid-flow dependent and flow-independent viscoelasticity (section 1.2.1). In a poroviscoelastic model both types of viscoelasticities are included (DiSilvestro and Suh 2001; DiSilvestro et al. 2001b,a; Suh and Bai 1998; Wilson et al. 2005a,b). Two different poroviscoelastic models can be found in the literature. In the first, the solid matrix is only viscoelastic in shear (DiSilvestro and Suh 2001)and in the second the solid matrix is viscoelastic both in shear and bulk deformation (Suh and Bai 1998). The solid stress of these models is given by

$$\sigma_E = \lambda e I + 2\mu \int_0^t G(t-\tau) \frac{\partial e}{\partial \tau} d\tau \tag{2.17}$$

and

$$\sigma_E = \lambda \int_0^t G(t-\tau) \frac{\partial eI}{\partial \tau} d\tau + 2\mu \int_0^t G(t-\tau) \frac{\partial e}{\partial \tau} d\tau \tag{2.18}$$

respectively. Here τ is a relaxation time constant and e is the deviatoric component of the elastic strain tensor. The relaxation function $G(t)$ is given by DiSilvestro and Suh (2001)

$$G(t) = 1 + \int_0^\infty S(\tau) e^{-t/\tau} d\tau \tag{2.19}$$

where the continuous relaxation spectrum $S(\tau)$ is given by

$$\begin{array}{ll} S(\tau) = c/\tau & \text{for} \quad \tau_1 \leq \tau \leq \tau_2 \\ S(\tau) = 0 & \text{otherwise} \end{array} \tag{2.20}$$

where τ_1 and τ_2 are the short and long term relaxation time constants, respectively, and c is the magnitude of the relaxation power spectrum. In addition to the biphasic material parameters in the isotropic case, the poroviscoelastic model adds three more parameters, which are a discrete spectrum value c, a short-term relaxation time constant τ_1 and a long-term relaxation time constant τ_2. The poroviscoelastic model is applied for the characterization of the time-dependent response of normal and degenerated cartilage in confined, and unconfined compressions and indentation.

2.1.8. *Other models*

In the isotropic and transversely isotropic models the material has the same properties in compression and tension. Isotropic conewise elasticity models take the compression-tension non-linearity of the tissue into account (Soltz and Ateshian 2000). Several other mechano-electrochemical models are also developed that include the influence of ion concentration and ion fluxes to represent the cartilage swelling behavior (Lai et al. 1991, 1993; Wilson et al. 2005a,b).

2.1.9. *Finite element formulation of biphasic theory*

The numerical complexity of the biphasic theory limited its applications to only those problems whose analytical solutions are readily derivable from the governing equations. These in general consisted of simple discs in confined compression. Solutions to more complex problems like in-vivo tissues and contact problems with realistic geometries are generally ushered in by the finite element formulations of the biphasic theory. Mow et al (1980); Oloyede and Broom (1991); Simon (1992) developed poroelastic finite element models for soft tissues and established the equivalence between the biphasic theory and poroelastic codes of soil mechanics (consolidation theory). Recently, the isotropic elastic biphasic theory saw many modifications by many researchers (Soulhat et al. 1999; Wilson et al 2003; Wilson et al. 2004, 2005a; Chen et al. 2006; Julkunen et al. 2007; Pawaskar et al. 2007) to include a more general anisotropy, fibril-reinforced, poro-viscoelastic and contact formulations.

Thus, over the past three decades, from the simple creep indentation tests by Hayes et al. (1972) to complex 3D finite element models by Wilson et al. (2005a), the advancements in the characterization of soft tissues like articular cartilage has been tremendous.

2.1.10. *Concluding remarks from constitutive models of cartilage*

We can conclude that the requirements of a material model are highly dependent on the research question to be answered. In general, the more features of the composition and structure of cartilage are included, the larger the number of material properties that must be estimated, and the more computationally expensive the model becomes. Hence, one should always try to use the simplest

model that is sufficient to obtain the required data. In this work, a metal implant to fill the degenerated cartilage is simulated in the sheep knee. Since, the cartilage thickness is very small (1 mm) compared to other joint dimensions (longest radius of condyle is 17.36 mm) in complex 3D geometry, it is enough to use simple isotropic biphasic model to capture the cartilage behavior surrounding the implant. Complex models, like fibril reinforced or poro-viscoelastic ones are not necessary for the research question to be answered in this work. Hence we adopted a simple isotropic poro-elastic biphasic model in ABAQUS.

Finite element analysis enables calculations of stresses and strains in the articular cartilage and also in the joint. It is useful in simulating the mechanical behavior of the cartilages surrounding the metal implant if it fills the local full thickness defects in the cartilage. We believe that FE modeling will help us to understand the effect of metal implant on the surrounding soft tissues and eventually provide tools for developing implant design.

2.2. Finite element modeling

The aim of this work is develop a numerical finite element (FE) model of a knee joint to study the mechanical behavior of cartilages with metal implants. The three dimensional finite element models were developed in general purpose finite element soft ABAQUS (Simulia, Inc., USA). Finite element modeling, generally, involves geometry, material representations and boundary conditions. These are briefly discussed in this section together with the poro-elastic model in ABAQUS.

2.2.1. *Poro-elastic model in ABAQUS*

The software package ABAQUS/Standard provides the capabilities for modeling fluid (wetting liquid) flow through a porous medium when the fluid is incompressible and the solid is completely saturated with the fluid. A porous medium is modeled in ABAQUS/Standard by the conventional poroelastic approach that considers the medium as a multiphase material and adopts an effective stress principle to describe its behavior (Hibbitt et al 2007).

The elementary volume (dV) in the porous medium is made up of a volume of solid material (dV_g) and a volume of wetting liquid (dV_w) that is free to move through the medium if driven. The basic variable in the fluid phase equations is the pore pressure, defined as the average pressure in the wetting liquid at a point in the porous medium. The total stress acting at a point, σ_{tot}, is assumed to be made up of an average pressure stress in the wetting liquid, p, and an effective stress, σ_E defined by Eq. (2.3).

The constitutive equation for the solid phase can be chosen to be of any form as long as it conforms to the restrictions on motion that are applied to a single phase material. The fluid phase constitutive response is modeled based on Darcy's law by Eq. (2.8).

The porous medium is modeled by attaching the finite element mesh to the solid phase and then liquid flow can be introduced through the nodes of the solid

mesh. The model also uses a continuity equation for the mass of wetting liquid in a unit volume of the medium together with general equilibrium equations for the solid phase. The permeability defined in the biphasic model (Mow et al 1980), k, was converted into that of the poroelastic model, k', through $k' = \gamma k$, where $\gamma = 9.81 \cdot 10^{-6}\mathrm{N/mm}^3$ is the volume weight of the interstitial fluid.

In ABAQUS, continuum pore pressure elements have a pore pressure degree of freedom in addition to the conventional displacement degrees of freedom. The poroelastic model in ABAQUS requires permeability to be specified as a function of the void ratio along with the elastic constants (Young's modulus and the Poisson ratio). Transient coupled pore fluid diffusion and stress analysis was adopted to analyze fully saturated porous media. Unsymmetric equations can follow from the contact between porous cartilages. Specifying use of the unsymmetric solver can sometimes improve convergence in this case. We used automatic time incrementation, as the time increments in a typical diffusion analysis can increase by several orders of magnitude during the simulation, by specifying a parameter (UTOL).

The integration procedure used in ABAQUS/Standard for consolidation analysis introduces a relationship between the minimum usable time increment and the element size, valid for fully saturated flow.

$$\triangle t > \frac{\gamma_w(1+\beta_w v^f)}{6Ek}\left(1-\frac{E}{K_g}\right)^2(\triangle l)^2 \tag{2.21}$$

where $\triangle t$ is the time increment, γ_w is the weight of the wetting liquid, E is the Young's modulus of the solid phase, k is permeability of the solid phase, v^f is the magnitude of velocity of pore fluid, β is the velocity coefficient in Forchheimer's flow law ($\beta = 0$ in the case of Darcy flow), K_g is the bulk modulus of the solid grains, $\triangle l$ is a typical element dimension.

If time increments smaller than these values are used, spurious oscillations may appear in the solution. If the problem requires analysis with smaller time increments, a finer mesh is required. The accuracy of the time integration of the flow continuity equations is governed by the maximum wetting liquid pore pressure change, $\triangle {u_w}^{max}$, allowed in an increment.

2.2.2. *Geometrical representation*

Since, the knee has a complex structure, constructing a simplified geometry is quite difficult. However, the femoral condyles of the knee can be approximated as simple ellipsoids if the whole joint is considered for an axial loading situation. Due to the symmetry between medial and lateral femoral condyles, modeling of one of them would be sufficient to capture the whole knee joint behavior. The proximal end of the tibial bone (tibial plateau) looks like an almost flat surface coated with a layer of cartilage. But, the menisci between the cartilages improve the congruency between the incongruent articular cartilages to evenly distribute the loads across the joint (Walker and Erkman 1975), by increasing

the contact area between the articulating surfaces in the joint (Wilson et al 2003).

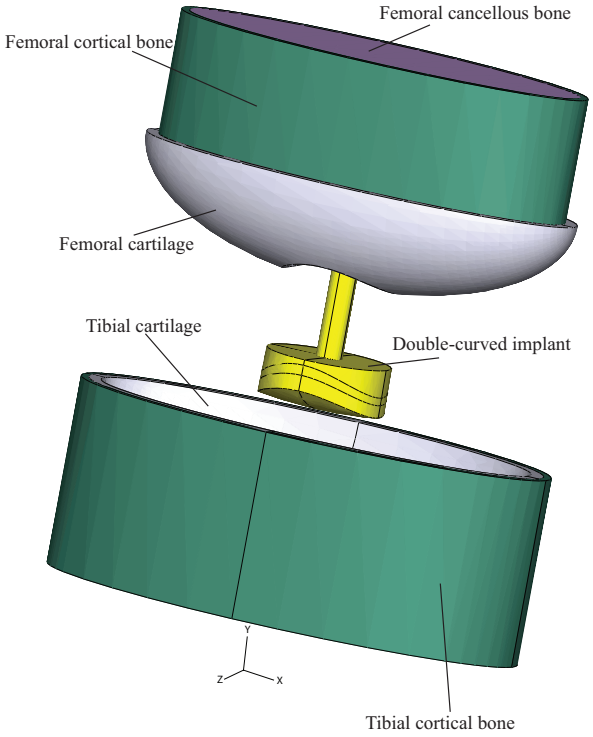

FIGURE 2.1. The simplified 3-dimensional geometrical representation of one of the condyles of the sheep knee joint with the established full thickness defect in the cartilage and a metal implant to fill the defect

.

However, the meniscus was not considered, due to lack of its complex geometrical details and to avoid difficulties in contact modeling in the numerical model. The meniscus was, however, indirectly introduced by assuming the contact surfaces perfectly congruent (idealized joint). Hence, the tibial plateau was assumed to be congruent with the femoral condyle, so the articular cartilages covering distal femoral and proximal tibial ends. Since, we mainly focussed on the cartilages immediately surrounding the implant, this assumption has only a limited effect on the results from the model. Poro-elastic formulation in ABAQUS requires initial conditions, like pore pressure and void ratio to be specified. The initial void ratio was here chosen as 4, and initial pore fluid pressure was assumed to be 600 Pa.

A simplified 3-dimensional representation of the sheep knee was developed, Fig. 2.1, by approximating one of the condyles of the sheep knee as semi-ellipsoid, and including cortical and cancellous parts of the bones. The dimensions were measured from a cadaveric sheep knee[1]. A circular hole in the cartilage representing idealized cartilage defect was assumed at the center, i.e., at load bearing area. The implant adopted in the model was developed at Episurf Medical AB, Stockholm for insertion into small full thickness cartilage defects in the sheep model. Later, the implant design will be extended to the human knee. A wedge shape was considered for the implant hat such that the circumference of the implant would increase when inserted into the cartilage defect. Thereby, it was planned to facilitate a mechanical sealing effect at the site of damage in the cartilage, so that further degeneration of cartilage can be prevented. The implant cap surface (articulating surface) was modeled with two profiles; a unicurved, spherical profile and double-curved profile. The latter matches exactly the articulating cartilage surface, when implant is positioned in-flush in the unloaded state. The depth at which the implant to be positioned was defined as the distance between the peak point of implant's cap and the corresponding point on the (removed) femoral cartilage surface at the defect site. Axial position of implant '+ x mm' represents an insertion of implant x mm deep into the femoral cartilage

The parametric study was conducted using the developed finite element models by varying defect size, implant's position with respect to cartilage surface, and wedge angle of the implant. The time dependent behavior of cartilages under high load for one hour was also simulated.

2.2.3. *Materials and boundary conditions*

The articular cartilages were modeled as biphasic materials (poro-elastic in ABAQUS) including strain dependent permeability and all other bones and the implant were modeled with isotropic elastic materials. The femoral bone was assumed to be fixed and the tibial bone was subjected to a load of 1 BW on one condyle (i.e., 2 BW on the whole knee, Taylor et al (2006)) in the form of pressure on the bottom surface of the model. A frictionless small sliding contact formulation was used between between the respective contact surfaces in the model[2].

In the biphasic poro-elastic medium, the load is shared by both fluid and solid phases (Mow et al 1980). Hence, the total contact pressure calculations should involve contributions from both fluid and solid. All of the contact pair options and all the contact property models that are pertinent to the pure mechanical contact interaction can be used for the coupled pore fluid-mechanical interaction. The pore fluid contact property models ensure continuity of the pore pressures on opposite sides of a contact interface at all times: $p_A - p_B = 0$, where p_A and p_B are pore pressures at points on opposite sides of the interface.

[1] more details are available in the appended papers

[2] Extended information about materials and boundary conditions is presented in the papers

ABAQUS/Standard assumes that pore fluid does not flow tangentially along the interface. In transient analysis the flow into the interface is balanced with the rate of separation of the two surfaces.

Hence, the contact pressure (CPRESS) between the two porous cartilages is effective, i.e., it does not take into account the pore fluid pressure. But, in case of contact between a porous cartilage and a impermeable metal implant, the contact pressure is total; i.e., it includes both effective structural and pore fluid pressure contributions (Hibbitt et al 2007).

The total pressure for all models, with or without implant, was obtained by using an impermeable membrane between the porous cartilages. The properties of membrane were chosen as Young's modulus, $E = 1$ MPa, Poisson ratio, $\nu = 0.5$ and thickness=0.01 mm (Wilson et al 2003). In diarthrodial joints, at the opposing surfaces of cartilages in contact, the fluid pressures will be very similar and the membrane has a limited effect on the results (Wilson et al 2003).

The analysis was divided into three different steps. In the first step, the implant inserts into the defect by means of removing interference between the implant and its surrounding femoral cartilage-cortical bone interface. In the second step, the contact establishes between cartilages. In the final step, the load is applied on the bottom plane of the tibia.

CHAPTER 3

Results and discussion

3.1. Results

The mechanical behavior of the cartilages surrounding an implant is characterized by contact pressures, displacements, stresses and fluid parameters determined at the defect edge. Some of these are presented in this section.

3.1.1. *Contact parameters*

The maximum contact pressure for healthy and untreated defect models were determined to compare the models with spherical or double-curved implants. The lowest maximum contact pressure was observed for all models when the implant was positioned slightly sunk into the cartilage based on the defect size[1]. Such example is shown for a 10 mm defect model after 120 s of constant load in Fig. 3.1. For a 10 mm defect model, the lowest maximum contact pressure was observed when the implant was positioned at + 0.1 mm. In the Fig. 3.1, 'healthy' refers to a case with undisturbed cartilage, and 'defect' to a case where cylindrical portion of a specific size is removed from it, with no implant introduced.

A double-curved implant, generally, showed lower contact pressures than a spherical implant in all the models. The reason for this is that the double-curved implant perfectly reproduces the articular surface in the joint because of its dual curvature. The spherical implant does not approximate the articulating surface due to its unicurved nature. In addition, spherical implant sits slightly sunk into the cortical bone in the antero-posterior plane, leaving some parts of the cartilage edge completely uncovered by the implant. The maximum contact pressures in the joint for various defect sizes are shown in Table 3.1 with the various positions of double curved implant.

The contact force transmitted through the implant was expressed as a percentage of the applied load, Fig. 3.2. With the implant positioned in flush, the opposing tibial cartilage is perfectly in contact with the implant even in the unloaded state. For implant positioned slightly sunk into the cartilage, the implant and opposing tibial surface come in contact as the time increases. The force transmitted through the implant increased to 10 %, 17 %, 25 % and 37% after 1 h of loading for 6, 8, 10 and 12 mm defect sizes, respectively, with the

[1]The extended results are presented in paper 1

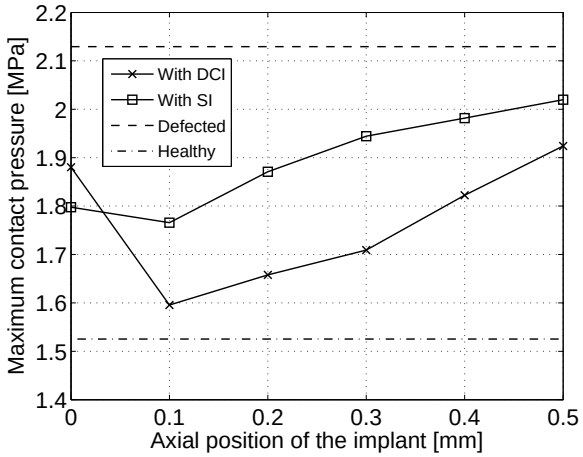

FIGURE 3.1. Maximum contact pressures in the 10 mm defect model at 120 s after full constant load (1 BW on one condyle). DCI: Double-curved implant, SI:Spherical implant.

TABLE 3.1. The maximum contact pressures [MPa] in the joint when different defect sizes filled with double-curved implant for various positionings

.

	Maximum contact pressures in the joint [MPa]			
	6 mm defect	8 mm defect	10 mm defect	12 mm defect
Healthy joint	1.525	1.525	1.525	1.525
Untreated defect	1.702	1.892	2.129	2.427
at + 0.0 mm	1.749	1.829	1.860	1.846
at + 0.1 mm	1.610	1.618	1.595	1.574
at + 0.2 mm	1.559	1.621	1.658	1.672
at + 0.3 mm	1.548	1.571	1.709	1.859
at + 0.4 mm	1.565	1.677	1.822	1.997
at + 0.5 mm	1.582	1.730	1.924	2.124

implant positioned at + 0.3 mm. The time dependent behavior[2] was studied for a time period of 1 h in the simulations.

3.1.2. *Displacements*

The axial compressions (average of the nodes on the defect edge) of both cartilages immediately surrounding the implant were determined with time. With the double-curved implant positioned at 0 mm, the axial compressions

[2]Many other results explaining time dependent behavior of cartilages was presented in the paper 2

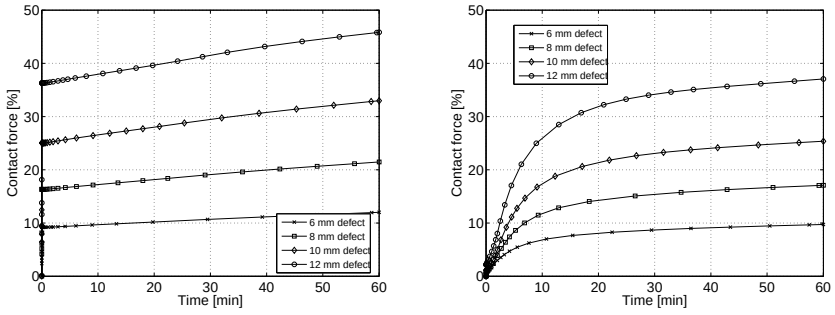

(a) (b)

FIGURE 3.2. The contact force transmitted through the implant-tibial cartilage interaction and expressed as the percentage of applied load, with double-curved implant positioned (a) at + 0 mm and (b) at + 0.3 mm.

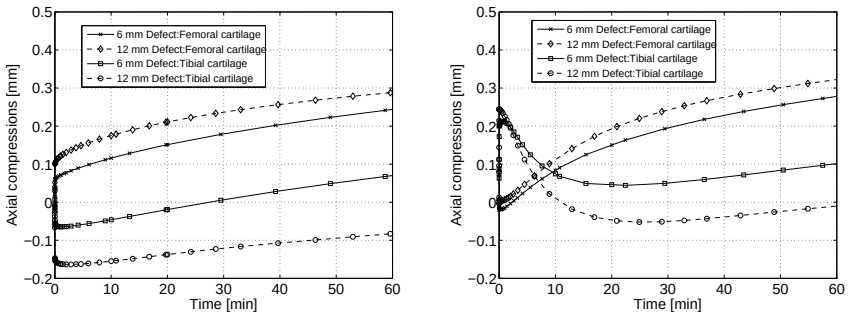

(a) (b)

FIGURE 3.3. Axial compressions of cartilages immediately surrounding the implant with double-curved implant positioned (a) at 0 mm and (b) at + 0.3 mm

.

of femoral edge were 24% and 28 % for 6 and 12 mm defects sizes, respectively, after 1 h of full constant load, Fig. 3.4. With the implant positioned at +0.3mm+ 0.3 mm, the compressions at femoral cartilage edge at the defect were increased to 27 % and 32 % after 1 h of constant load from zero for 6 and 12 mm defect sizes, respectively. During the early period of load application, the portion of tibial cartilage surrounding the implant was compressing more than the corresponding femoral edge. As time progressed, this was reversed until the implant-tibial cartilage interface starts transmitting load. Then onwards, as the time progresses, the compressions in both cartilages around the implant were increasing.

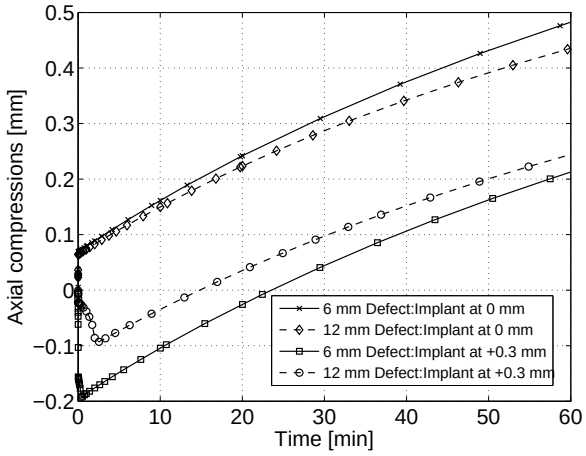

FIGURE 3.4. Axial compressions at center point of the tibial cartilage facing the implant.

The compression at the center point of opposing tibial cartilage was increased to 48 % and 43 % after 1 h of loading with the double curved implant positioned at 0 mm. With the implant at + 0.3 mm, the center point of tibial cartilage expands intially, but as time progresses, the implant comes in contact with the tibial surface, resulting in increased compression at the interface, Fig. 3.4. These compressions increased to 21 % and 24 % after 1 h of loading for 6 and 12 mm defect sizes, respectively.

3.2. Discussion

Despite the introduction of new biological and surgical techniques, the treatment of full thickness chondral defects remains challenging. Experimental studies showed the possibility of using metal implants to treat such defects as an alternative to the available biological repair methods. However, the mechanical effect of the implant on its surrounding is not clearly known, driving us motivated. The goal of the present study was, intially, to develop a conceptual poro-elastic finite element model for the sheep knee to simulate the mechanical behavior of the cartilages surrounding a metal implant filling a full thickness cartilage defect. Subsequently, our aim was to investigate the various parameters that affect the mechanical behavior of surrounding cartilage, like position, size, wedge angle and articulating shape of the implant. Contact pressures, contact forces, displacements and stresses were considered as the measures of the mechanical behavior in the joint.

Many finite element studies are performed on osteochondral defect repair and healing (Smith and Mansour 2000; Duda et al. 2005; Peña et al 2007). Condiering a metal implant to fill the defect site has never been studied before, as far as we know. The double-curved implant gave the lower contact pressures

and stresses in the cartilage edges than for a spherical one. Hence, we conclude that a double-curved implant is better suited than a spherical one for treating the defects in the cartilage. The sticking up of the implant into the joint cavity may damage the opposing tibial cartilage during rapid dynamic movements of the knee. Hence, determining the deformations in the cartilages immediately surrounding the implant are necessary to predict the protrusion of implant into joint cavity.

Since, the time dependent behavior of the cartilages is well studied in the literature, we wanted to study the same when the metal implant fills the defect in the cartilage. From the simulations, we observed a significant effect of time on the results. The cumulative effect of a cyclic load, simulating normal gait, was reflected by a constant static load for a long time (one hour). Here, we raised a question about what could be the optimum time point at which the results should be considered as primary. We believe that neither very short time nor too long time is appropriate to represent the correct and physiologically relevant results. The results after 60 s of full constant loading may be a reasonable choice. We also observed that mechanical sealing effect due to the wedge shape of the implant is significantly dependent on time. When the implant positioned slightly sunk into the cartilage, the sealing effect (quantified by reduction in permeability) was increasing with time.

Using small displacement formulation for solving equations from the contact modeling between the cartilages is a reasonable choice, because there exists very little relative motion between surfaces that come into contact in the joint, in particular for the axial loading considered in the models. The displacement control was used only to establish the contact to avoid convergence difficulties. Force control was then used in the simulations when applying a load in the form of pressure on the bottom plane of the tibia.

The main limitations of the present study include the geometry and loading case considered. Firstly, the geometry is an approximation based on the rough measurements from a cadaveric sheep knee. We believe that this approximation is quite reasonable for the axial loading case considered, and relevant if, as development seems to be heading, implants to be individually measured and manufactured. Further, the meniscus was not considered. We are aware that the meniscus, transmits the load more evenly in the joint, makes the joint congruent (Walker and Erkman 1975), but not into the totally idealized joint modeled in this work. We, however, believe that, in the vicinity of the defect considered (i.e, at the load bearing area), the joint articulating surfaces are perfectly congruent due to meniscus. Hence, the removal of this meniscus, by considering idealized geometry, has a very limited effect on the results obtained as we mainly focussed on the behavior of cartilages immediately surrounding the defect site, i.e., around the implant. In order to simulate non-axial and/or dynamic loadings on the model, geometry needs to be modified. The isotropic

properties considered in the model are quite reasonable for the research questions that were answered from the present model. Finally, the material properties used for the modeling of the cartilages in the model are from human models due to the lack of cartilage properties in the sheep. We believe that a sheep model has properties close to human, due to its validation as a large animal model in orthopaedics by many researchers Zarrinkalam et al. (2009); Martini et al. (2001).

The model can be easily modified to accommodate different defect sizes and implants. The data determined in the study may have important implications in the ongoing animal experiments in the sheep model (Episurf Medical AB, Stockholm, Sweden), and in the future development of human implants.

CHAPTER 4

Summary of papers

4.1. Paper 1

Finite element simulations of a focal knee resurfacing implant applied to localized cartilage defects in a sheep model

The main aim of the paper is to develop a conceptual finite element model to simulate the articular cartilage behavior surrounding a metal implant when it fills a full thickness cartilage defect in the knee. For this purpose, a simple 3-dimensional geometrical representation was made for a sheep knee joint. One of the femoral condyles of the knee can be approximated as semi ellipsoid if an axial loading situation is considered. Hence, a geometry was developed based on the measurements on a cadaveric sheep knee. A defect was established on the load bearing area and expressed as a circular hole with specific size. Two types of implants were developed to fill this assumed defect. One is a unicurved spherical profile and the other is a double-curved profile of a specific defect size. The simulations are performed in ABAQUS by considering poro-elastic material for cartilages and linear elastic materials for bones and implant. The double-curved implant which exactly matches the articulating surface gave lower contact pressures than the unicurved implant,. The effect of the implant's position on the surrounding is important to avoid sticking up of the implant into the joint cavity. Hence, a parametric study was conducted by changing axial position of the implant. From this, we found that the implant should be placed slightly sunk into the cartilage to avoid damage to the opposing articulating surface. We observed that with increasing defect size, the closer the implant should be to the flush. We also seen mechanically from the simulations that, using a metal implant to treat a full thickness defect in the cartilage is advantageous compared to leaving the defect untreated. A mechanical sealing effect was also observed with the wedge shaped implant. The contact pressures, deformations and stresses in the joint were the measures of the mechanical behavior of the cartilages.

4.2. Paper 2

Time dependent behavior of cartilages surrounding a metal implant for full thickness cartilage defects of various sizes: a finite element study

The main aim of this paper is to investigate the time dependent behavior of articular cartilages immediately surrounding the implant. For this purpose, the

model developed in paper 1 was used in simulations for a time period of 1200 s. We found that time plays a vital role in the behavior of cartilage surrounding the metal implant. We found the time dependent deformations, contact pressures in the cartilages with the implant positioned in flush and 0.3 mm sunk into the cartilage. The deformations in the cartilage edges surrounding the implant were increasing with time. For clinical interpretations, the results should be taken at neither very short time point nor very long time point, but an intermediate time point should be considered. The results after 60 s may, therefore, be treated as the primary results, reflecting the accumulated effect of short time cyclic loads. As time progresses, the load transfer through the implant between the bones is increasing even with the implant sunk 0.3 mm into the cartilage. The mechanical sealing effect can be quantified with the decrease in permeability (solidification of material) in the cartilage defect edge around the implant. This decrease in permeability slows down the fluid flow in the edge during dynamic movements, indicating possible mechanical sealing. With increasing wedge angle of the implant, this effect was shown to be increasing with time.

CHAPTER 5

In vivo loads acting at knee

The simulations being the main ingredients of this study were performed with a simple loading situation. As the loading situation in the knee joints is, however, very complex, a study of the real in vivo loading has been performed. A brief summary is given here.

The determination of in vivo forces and moments acting at the knee joint is important to investigate the loading mechanisms that cause degenerative joint diseases, to simulate the clinical orthopaedic surgery procedures, to estimate the survival of the implant, design of new implants, in total knee arthroplasty, and for improving and verifying analytical biomechanical models. This chapter aims at evaluating various techniques used to measure in vivo forces in the human knee joint. The in vivo force estimation can be divided into two broad categories; mathematical modelling and telemetry. The forces in the knee joint are often normalized with respect to the patient's body weight (BW).

5.1. Mathematical modeling

The mathematical modeling, which is a theoretical approach, requires some kinematic/kinetic data measured in vivo or in vitro. This data is inputted to the developed musculoskeletal/mathematical model and through inverse dynamics principles, the forces and moments can be determined at the joints. The analytical modeling of the human knee joint is quite difficult as it involves three rigid bones (tibia, femur and patella) which move in a complex way relative to each other, unlike any other joint in the human body. The presence of patellofemoral joint contribute to the difficulty in developing reliable models. A knee joint can be described with six interactive forces and 6 active moments (Komistek et al. 1998). The human leg is composed of numerous muscles which can be represented by many resultant forces and moments. These redundant forces make the system indeterminate. To solve this system, two methods are widely accepted; optimization and reduction techniques.

Seireg and Arvikar (1973, 1975) developed one of the first mathematical models for knee, based on optimization principles. Then, extensive work has been carried out by Crowninshield (1978); Crowninshield et al. (1976). A mathematical model, simulating human during normal walking, was developed by Anderson and Pandy (2001). Most of the models using optimization principles either overestimate or give physiologically inaccurate results (Brand et al.

1994; Challis 1997). In reduction technique, the number of unknowns is reduced compared to the number of equations. Researchers have chosen many forms of reduction methods (Komistek et al. 1998; Morrison 1970; Paul 1976; Wimmer and Andriacchi 1997). In all the models, the underlying assumption is that certain muscles do not affect the system significantly. Hence, it is unnecessary to include these muscles, or to group them together in order to reduce the number of unknowns in the system. Paul (1976) modeled the whole lower extremity and determined the forces at hip, knee and ankle joints for various activities using a reduction method. The models developed by Morrison (1970) is the most frequently cited in the literature, calculate the forces in ligaments, muscles and between the femur and tibia. Komistek et al. (1998) developed a model based on Kane's method and reported that the maximum tibiofemoral force was 1.7-2.3 times body weight depending on walking speed. Known variables inputted to their model are ground reaction forces, gravitational, inertial forces of the lower extremity and relative motions between bones measured using fluoroscopy. The maximum tractive force in the joint was calculated as 0.4 BW by Wimmer and Andriacchi (1997) using a mathematical model including friction. This model mainly focussed on sagittal plane motion of the femur on the tibia.

Taylor et al. (2004) developed a musculoskeletal model for lower extremity based on CT data to determine forces at the knee joint and gait analysis is performed on four patients to measure kinematics of knee and ground reaction forces. But, the soft tissues at the joint are not included in the model. By inverse dynamics, the forces at knee are predicted. The average anteroposterior peak shear components are 0.6 BW during walking and 1.3 BW during stair climbing. Kuster et al. (1997) estimate the muscle forces contribution to bone-on-bone forces at knee joint as 70% during level walking and 80% during downhill walking, whereas ground reaction forces contribution is 20% and 30%, respectively, using kinematic and kinetic measures and inverse dynamics principles.

Despite having distinct advantage of being parametric, mathematical modeling overestimates the loads at the joints, shows high variation between different studies and the uncertainties prevail in the models (Komistek et al. 2005).

5.2. Telemetry

The alternative to the mathematical modeling, to overcome its uncertainties, is a direct measurement by telemetrized implants. Telemetry, which is an experimental approach, uses force transducers, sensors fitted to a prosthetic component and video fluoroscopy, CT scanning, MR images to directly measure the in vivo contact loads, moments and kinematics after knee arthroplasty. Telemetric methods produce very accurate and direct measurements of forces and moments across the human joints, with the only inaccuracy due to an affected movement pattern after surgery. Usually, telemetric devices are very expensive and technically challenging, require implantation of the device into

the joint. Any wrong doing of the implant or malfunctioning of the sensors are irrevertible. For example, Davy et al. (1988) faced a malfunctioning of the telemetric implant between 31 and 45 days of the post-operative period. Telemetric methods have been successfully used to determine forces acting at the hip joint in the past (Bergmann et al. 2001, 2004), and, more recently evaluated the forces at the knee joint.

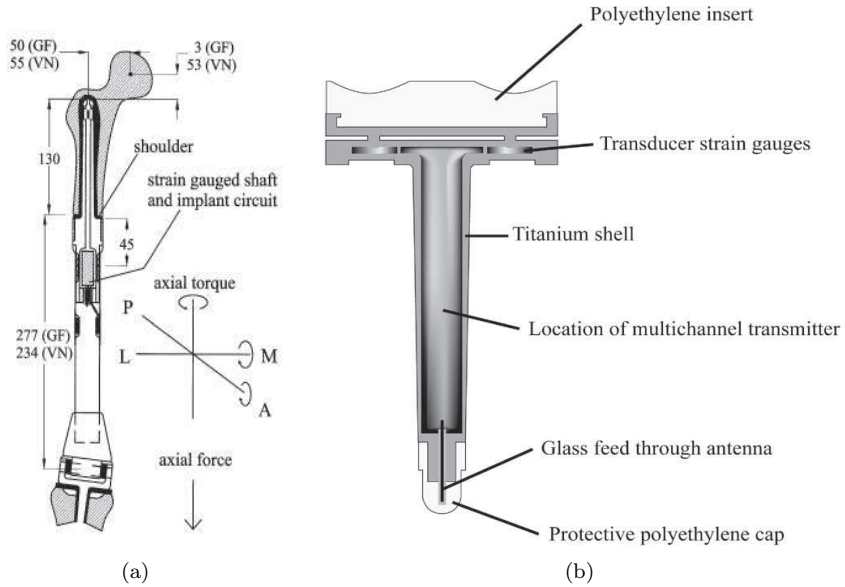

FIGURE 5.1. (a) Schematic illustration of the instrumented distal femoral replacement (anterior view) to measure in vivo axial forces in the knee joint. It was the first attempt to measure in vivo forces; reproduced from Taylor and Walker (2001), (b) Cross section of the instrumented tibial prosthesis. Reproduced from D'Lima et al. (2005)

.

The first group that extracted in vivo forces near the knee was Taylor et al. (1997, 1998); Taylor and Walker (2001). They measured the forces and moments in the shaft of an instrumented distal femoral replacement prosthesis (20 cm away from the knee) for a subject during different activities. Then, calculations were made to transfer the measured loads to knee joint line level using appropriate numerical models. Taylor et al. (1998) predicted peak axial force as 2.2 to 2.5 BW and shear force in the joint as 0.4 to 0.5 BW and also calculated patellofemoral force as 0.69 to 0.83 BW during level walking. A follow-up study was then conducted by Taylor and Walker (2001). They found that maximum forces at the knee joint during gait, jogging, stair descending and ascending as 2.8, 3.6, 3.1 and 2.8 BW, respectively. They also observed that

knee joint force is higher during level walking than during treadmill walking (2.75 BW), and that forces and moments during jogging are higher than those for other activities. The prosthesis was instrumented in the shaft, Fig. 5.1(a), to measure longitudinal axial force and torque, and two bending moments in antero-posterior (A-P) and medial-lateral (M-L) axes. The bending moments about A-P axis (varus-valgus) and M-L axis (flexion-extension) are in the range of 8.5-9.8 and 4.7-7.6 BW cm, respectively. The axial torque is in the range of 0.2-1.3 BW cm.

Kaufman et al. (1996) developed a customized transducer to measure the dynamic tibiofemoral forces and the center of pressure after total knee arthroplasty and verified their results in vitro. The transducer consists of a standard tibial component having four uniaxial load cells and an additional tibial tray. Burny et al. (2000) also developed an orthopaedic implant instrumented with strain gauges connected to a Wheatstone bridge by means of percutaneous leads.

Some years ago, an instrumented tibial baseplate (first generation of force-sensing device) was developed and tested in a cadaver knee, and then implanted into one subject, allowing the measurement of intra-articular axial tibial forces (D'Lima et al. 2005, 2006). This tibial prosthesis was instrumented with four force transducers located at the four quadrants of the tibial tray, Fig. 5.1(b), to measure the compressive tibial forces and the location of the center of pressure in the knee joint. The determined axial forces on the tibia are 2.2 BW in level walking and 1.9 to 2.5 in stair climbing. On the same subject, Mündermann et al. (2008); Zhao et al. (2007) examined the relationship among activity, peak load, medial to lateral load distribution, and flexion angle at peak load for daily activities. They observed that for all activities, the total compressive load exceeded 2 BW, and for most activities 2.5 BW. Most activities placed a greater load on the medial compartment than on lateral compartment. The percentage of medial to total contact force range from 18 to 60 % for gait, 47 to 65 % for step up/down, and 55 to 60 % for kneel and lunge (Zhao et al. 2007). In all the above findings in the paragraph, in vivo motion using fluoroscopy was collected simultaneously, measuring the axial loads using instrumented tibial prosthesis. D'Lima et al. (2008a) used these tibial forces and knee kinematic data collected in vivo to calculate contact stresses using finite element analysis. They modeled polyethylene insert as an elastoplastic material. The predicted contact stresses are validated using pressure sensitive sensors. Stair climbing generated higher contact stresses (32 MPa) than walking (26 MPa).

Recently, a second-generation force-sensing device that measures all six components of tibial forces has been developed, and load measurements using it, in up to three subjects are reported (Kirking et al. 2006; D'Lima et al. 2007, 2008b; Varadarajan et al. 2008). They measured peak total forces for various activities, Table 5.1, simultaneously measuring kinematics using a dual fluoroscopic imaging system. Peak anterior shear forces at the tibial tray were 0.30 BW during walking, 0.17 BW during chair rise, 0.26 BW during stair climbing,

and 0.15 BW during squatting. The measured peak flexion moment at the tray is 1.9% BW Ht (percentage of body weight multiplied by height) for chair-rising and 1.7 % BW Ht for squatting. Peak adduction moment at the tray was 1.1% BW Ht during chair-rise, 1.3% BW Ht during squatting. They also measured the knee forces and moments during exercise and recreational activities (D'Lima et al. 2008b). However, not all load components are reported, and the flexion-extension and varus-valgus moments are not reported for walking and stair climbing, which are indeed most frequent activities.

More recently, another group (Heinlein et al. 2009; Kutzner et al 2010; Heinlein et al. 2007) reported complete data from a total knee replacement loading, measured in up to five subjects using a sophisticated instrumented tibial tray, Fig. 5.2. The highest mean values of the peak load components during level walking (Heinlein et al. 2009) are 2.08 to 2.76 BW in axial direction, 0.21 BW in medio-lateral direction, and 0.29 BW in antero-posterior direction; the moments are 1.8% BW m in the sagittal plane, 4.3% BW m in frontal plane and 1.0% BW m in transversal plane. During stair climbing the axial force increased to 3.06 BW, while the shear forces changed slightly; the sagittal plane moment increased to 2.4% BW m, while the frontal and transversal plane moments decreased slightly. Stair descending produced the highest forces of 3.52 BW (axial), 0.35 BW (medio-lateral), and 0.36 BW (antero-posterior). The sagittal and frontal plane moments increased to 2.8% BW m and 4.6% BW m, respectively, while the transversal plane moment changed slightly. Kutzner et al (2010) measured the forces and moments in five subjects, and the reports that the highest moments act in the frontal plane, in the range of -2.91% BW m (adduction moment) to 1.61 % BW m (abduction moment) throughout all activities. Peak flexion/extension moments were between -0.44% BW m (extension moment) and 3.16% BW m (flexion moment). Peak external/internal torques were between -1.1% BW m (internal torque) and 0.53% BW m (external torque).

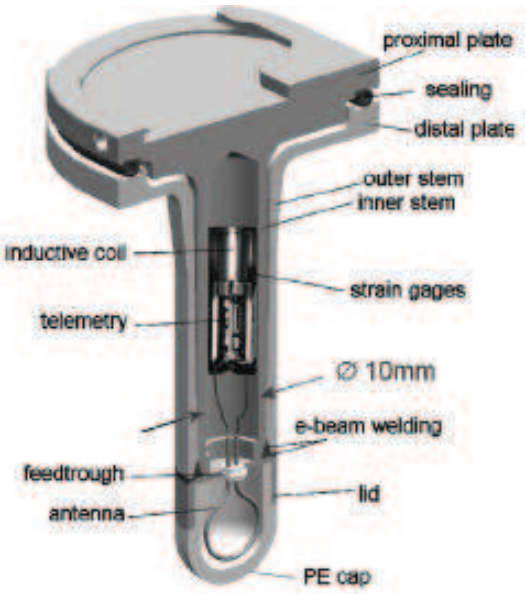

FIGURE 5.2. Cross section of instrumented tibial prosthesis. Reproduced from Heinlein et al. (2007)

Table 5.1: Comparison of the knee joint forces obtained from different approaches.

References	**Activity**	**Axial load (BW)**	**Technique**
Morrison (1970)	Walking	2.1 - 4.0	Reduction
Seireg and Arvikar (1973)	Walking	7.1	Optimization
Komistek et al. (1997)	Walking	1.7 - 2.3	Reduction
Wimmer and Andriacchi (1997)	Walking	3.3	Reduction
Paul (1976)	Walking Stair descending Stair ascending Up ramp Down ramp	2.7 - 4.3 4.9 4.4 3.7 4.4	Reduction
Komistek et al. (2003, 2005)	Walking Deep knee bending	2.1 - 3.4 1.8 - 3.0	Reduction
Taylor et al. (2004)	Walking Stair ascending	3.1 5.4 - 6.2	Musculoskeletal model
Kuster et al. (1997)	Level Walking Downhill walking	3.9 8	Kinematics/inverse dynamics
Thambyah et al. (2005)	Walking	2.8 - 3.2	Musculoskeletal model
Taylor et al. (1998)	Level walking Stair ascending Stair descending Chair rising Standing on one leg Lying supine and raising the leg	2.2 - 2.5 2.5 2.8 2.0 2.4 1.7	Telemetry
Taylor et al. (1999); Taylor and Walker (2001)	Jogging Stair ascending Stair descending Level walking	3.6 2.8 3.1 2.8	Telemetry

Continued on next page...

References	**Activity**	**Axial load (BW)**	**Technique**
	Treadmill walking	2.75	
D'Lima et al. (2006)	Walking	2.2	Telemetry
	Stair ascending	1.9 - 2.5	
Zhao et al. (2007)	Treadmill gait	2.2	Telemetry
	Step up/down	3.5	
	Kneel	0.2 - 0.4	
	Lunge	1.2 - 2.2	
D'Lima et al. (2007)	Walking	2.3	Telemetry
	Chair rising	2.5	
	Stair climbing	3	
	Squatting	2.1	
Heinlein et al. (2007)	Lunge	2.76	Telemetry
	Stair climbing	3.06	
	Stair descending	3.52	
Varadarajan et al. (2008)	Lunge	2.24	Telemetry
	Chair sitting-rising	1.87	
Kutzner et al (2010)	Stair descending	3.46	Telemetry
	Stair ascending	3.16	
	Level walking	2.61	
	One legged stance	2.59	
	Knee bending	2.53	
	Standing up	2.46	
	Sitting down	2.25	
	Two legged stance	1.07	
	Deep knee bending	1.8 - 3.0	

A review of all techniques provide wide ranges of measured forces during various activities. This chapter summarizes all force data at the knee, briefly explaining mathematical modeling and telemetered techniques from the literature. A review of all the techniques to measure the in vivo loads at the knee joint, reveals a wide range of forces 0.2 to 8 BW, summarized in Table 5.1 for various activities. In general, resultant contact forces measured from direct measurement techniques (telemetry) during dynamic activities are more accurate and lower than the ones predicted by many mathematical models. However, telemetry is restricted in its use because of the high costs involved in

developing a instrumented implant, and because they require a surgery and a willing subject.

CHAPTER 6

Conclusions and future work

6.1. Conclusions

A simplified 3-dimensional geometrical representation of a sheep knee condyle was created. Using this representation, the mechanical behavior of the cartilages surrounding a metal implant filling the full thickness cartilage defect was investigated by finite element methods. Our study strengthens the idea of using a metal implant to fill such chondral defects, thereby reproducing articulating surface in the knee joint. We observed that, filling the full thickness chondral defects with metal implants is always more advantageous than leaving them untreated from a mechanical point of view. The double-curved implant fully congruent with articulating surface is preferable to a unicurved spherical profile, as the contact pressures and stresses are lower than for a spherical one. The implant placed slightly sunk into the cartilage gave the lowest maximum contact pressure in the joint based on the defect size. We observed that the larger the defect size, the closer the implant's surface should be to the flush in order to produce lower contact pressures in the joint. We found maximal deformations, stresses and contact pressures in the joint when the metal implant replaces the degenerated portion of the cartilage. The deformations determined at the defect edge of the cartilages were instrumental in order to avoid the protrusion of implant, which may damage the opposing soft tissues.

The time dependent behavior of the cartilages surrounding the implant was also simulated for an hour of constant loading. We conclude that time has a significant effect on the results obtained in the present work. The reason for this can be explained by complex fluid movement in the poro-elastic model over time. The main purpose of the implant was to seal the surrounding cartilage at the defect. This was achieved mechanically, beside the biological sealing, by a wedge shape of the implant cap. The mechanical sealing was quantified in terms of reduction in fluid permeability at the defect edge surrounding the implant. This was shown to be increasing with wedge angle as well as with time. The developed model in the present work is a simulation tool and was validated qualitatively with the preliminary experiments on a sheep model (Episurf Medical AB, Stockholm). Different defect sizes and implants can be easily incorporated into the model. The model has a potential, in relevant aspects, to predict the physiological behavior of the cartilages immediately surrounding the implant.

6.2. Future work

From an extensive literature review on the loads acting at knee joint, one could think of more realistic loading patterns to be applied in the simulations. The simulations performed in this work have not included any non-axial loadings or dynamic cyclic loadings on the joint, relevant for a human knee subjected to during daily activities. Further, model improvements can be done to include these various loading situations. The sheep knee geometry assumed in this work is mainly suited for the axial loading case considered. In order to incorporate the dynamic loading, geometry has to be modified accordingly. This model will be extended to more general human knee by including necessary elements of the knee. The constitutive models used for the modeling of articular cartilage can be further improved to capture an even more realistic time dependent behavior of the joint.

From a vast literature review of the behavior of cartilages, we found a gap in the literature about in vivo time dependency of articular cartilage. Few researchers have attempted to observe the deformational behavior of cartilages in vivo, mainly focussing on the in vitro studies or a single body weight load. Magnetic resonance imaging ('MRI') techniques can be utilized to capture the cartilage behavior during heavy weight bearing applications, especially during the first few minutes of the load. We are looking forward to design an experimental set up (mechanical point of view) to apply heavy loads on the knee in an MRI scanner and to measure experimentally the deformational behavior of cartilage. The same will be numerically modeled and verified.

The understanding of the mechanics of biological joint from the extensive literature survey could be helpful to simulate the same in a load carrying system in an engineering example. The similarities in the kinematics and kinetics of joints can then be compared between the biological and engineering load carrying structures.

Acknowledgements

I would like to express my sincere gratitude to my advisor, Prof. Anders Eriksson, for giving me the opportunity to work in his research group as a post-graduate student, and his guidance, enthusiasm, vast knowledge of mechanics, which has been invaluable throughout the course of this thesis. Without his personal assistance and moral support, this work would have not been in this shape. I am greatly indebted to him.

I render my sincere thanks to Prof. Leif Ryd for posing some clinical questions regarding this project which drove us motivated. I wish to express my thanks to the company Episurf Medical AB, Stockholm for providing necessary data for model development and also for giving me the opportunity to participate in their Big group meetings.

I wish to thank the people at the Department of Mechanics, KTH, especially to my research group members for providing a friendly working environment. A special thank goes to Robert and Seif (colleagues in the same office) whose company and help were invaluable during the last two years. Many thanks to all my well-wishers who supported me on my difficult times and guided me to the engineering world.

My parents and sisters receive my deepest gratitude for their many years of love and support. Many thanks to my corridor mate, Bhupesh Reddy, for providing a friendly environment in the corridor where I live and, of course, his assistance in cooking every day is greatly acknowledged. Lastly, I am greatly indebted to Arun Bharath Vadde, without whose constant moral support since 2003, neither me nor this work would have been the same.

Bibliography

Akizuki, S., Mow, V. C., Muller, F., 1986. Tensile properties of human knee joint cartilage: I. influence of ionic conditions, weight bearing, and fibrillation on the tensile modulus. Journal of Orthopaedic Research 4 (4), 379–392.

Anderson, F. C., Pandy, M. G., 2001. Dynamic optimization of human walking. Journal of Biomechanical Engineering 123 (5), 381–390.

Ashman, R. B., Rho, J. Y., Turner, C. H., 1989. Anatomical variation of orthotropic elastic moduli of the proximal human tibia. Journal of Biomechanics 22 (8-9), 895–900.

Ateshian, G. A., Ellis, B. J., Weiss, J. A., 2007. Equivalence between short-time biphasic and incompressible elastic material responses. Journal of Biomechanical Engineering 129 (3), 405–412.

Ateshian, G. A., Warden, W. H., Kim, J. J., Grelsamer, R. P., Mow, V. C., 1997. Finite deformation biphasic material properties of bovine articular cartilage from confined compression experiments. Journal of Biomechanics 30 (11-12), 1157–1164.

Bae, W. C., Sah, R. L., 2008. Multi-scale biomechanics of articular cartilage. An introductory text to bioengineering, Editors: Chien,S. and Chen,P. C. Y. and Fung, Y. C., Advanced secried in biomechanics- vol. 4, World scientific publishers, 243–260.

Becher, C., Huber, R., Thermann, H., Paessler, H. H., Skrbensky, G., 2008. Effects of a contoured articular prosthetic device on tibiofemoral peak contact pressure: A biomechanical study. Knee Surgery,Sports Traumatology,Arthroscopy 16 (1), 56–63.

Becher, C., Huber, R., Thermann, H., Tibesku, C. O., von Skrbensky, G., 2009. Tibiofemoral contact mechanics with a femoral resurfacing prosthesis and a non-functional meniscus. Clinical Biomechanics 24 (8), 648–654.

Bergmann, G., Deuretzbacher, G., Heller, M., Graichen, F., Rohlmann, A., Strauss, J., Duda, G. N., 2001. Hip contact forces and gait patterns from routine activities. Journal of Biomechanics 34 (7), 859–871.

Bergmann, G., Graichen, F., Rohlmann, A., 2004. Hip joint contact forces during stumbling. Langenbeck's Archives of Surgery 389 (1), 53–59.

Brand, R. A., Pedersen, D. R., Davy, D. T., Kotzar, G. M., Heiple, K. G., Goldberg, V. M., 1994. Comparison of hip force calculations and measurements in the same patient. Journal of Arthroplasty 9 (1), 45–51.

Brittberg, M., Aglietti, P., Gambardella, R., Hangody, L., Hauselmann, H. J., Jakob, R. P., 2000. Cartilage injury evaluation package. ICRS Cartilage Injury Evaluation Package.

Brittberg, M., Lindahl, A., Nilsson, A., Ohlsson, C., Isaksson, O., Peterson, L., 1994. Treatment of deep cartilage defects in the knee with autologous chondrocyte transplantation. New England Journal of Medicine 331 (14), 889–895.

Brown, T. D., Ferguson Jr., A. B., 1980. Mechanical property distributions in the cancellous bone of the human proximal femur. Acta Orthopaedica Scandinavica 51 (3), 429–437.

Brown, T. D., Pope, D. F., Hale, J. E., Buckwalter, J. A., Brand, R. A., 1991. Effects of osteochondral defect size on cartilage contact stress. Journal of Orthopaedic Research 9 (4), 559–567.

Buckwalter, J. A., Mankin, H. J., 1998. Articular cartilage: degeneration and osteoarthritis,repair,regeneration,and transplantation. Instructional course lectures 47, 487–504.

Burny, F., Donkerwolcke, M., Moulart, F., Bourgois, R., Puers, R., Van Schuylenbergh, K., Barbosa, M., Paiva, O., Rodes, F., Bégueret, J. B., Lawes, P., 2000. Concept,design and fabrication of smart orthopedic implants. Medical Engineering and Physics 22 (7), 469–479.

Challis, J. H., 1997. Producing physiologically realistic individual muscle force estimations by imposing constraints when using optimization techniques. Medical Engineering and Physics 19 (3), 253–261.

Chen, A. C., Bae, W. C., Schinagl, R. M., Sah, R. L., 2001. Depth- and strain-dependent mechanical and electromechanical properties of full-thickness bovine articular cartilage in confined compression. Journal of Biomechanics 34 (1), 1–12.

Chen, X., Chen, Y., Hisada, T., 2006. Development of a finite element procedure of contact analysis for articular cartilage with large deformation based on the biphasic theory. JSME International Journal, Series C: Mechanical Systems, Machine Elements and Manufacturing 48 (4), 537–546.

Cohen, B., Gardner, T. R., Ateshian, G. A., 1993. The influence of transverse isotropy on cartilage indentation behavior - a study of the human humeral head. Trans. Orthop. Res. Soc. 18, 185.

Cook, R. D., Malkus, D. S., Plesha, M. E., Witt, R. J., 2002. Concepts and applications of finite element analysis. Fourth edition, John Wiley & Sons, Inc,NY.

Crowninshield, R., Pope, M. H., Johnson, R. J., 1976. An analytical model of the knee. Journal of Biomechanics 9 (6), 397–405.

Crowninshield, R. D., 1978. Use of optimization techniques to predict muscle forces. Journal of Biomechanical Engineering 100 (2), 88–92.

Curl, W. W., Krome, J., Gordon, E. S., Rushing, J., Smith, B. P., Poehling, G. G., 1997. Cartilage injuries: A review of 31,516 knee arthroscopies. Arthroscopy 13 (4), 456–460.

Currey, J. D., 1988. The effect of porosity and mineral content on the Young's modulus of elasticity of compact bone. Journal of Biomechanics 21 (2), 131–139.

Custers, R. J. H., Creemers, L. B., van Rijen, M. H. P., Verbout, A. J., Saris, D. B. F., Dhert, W. J. A., 2009a. Cartilage damage caused by metal implants applied for the treatment of established localized cartilage defects in a rabbit model. Journal of Orthopaedic Research 27 (1), 84–90.

Custers, R. J. H., Creemers, L. B., Verbout, A. J., van Rijen, M. H. P., Dhert, W. J. A., Saris, D. B. F., 2007a. Reliability,reproducibility and variability of the traditional histologic/histochemical grading system vs the new OARSI osteoarthritis cartilage histopathology assessment system. Osteoarthritis and Cartilage 15 (11), 1241–1248.

Custers, R. J. H., Dhert, W. J. A., Saris, D. B. F., Verbout, A. J., van Rijen, M. H. P., Mastbergen, S. C., Lafeber, F. P. J. G., Creemers, L. B., 2010a. Cartilage degeneration in the goat knee caused by treating localized cartilage defects with metal implants. Osteoarthritis and Cartilage 18 (3), 377–388.

Custers, R. J. H., Dhert, W. J. A., van Rijen, M. H. P., Verbout, A. J., Creemers, L. B., Saris, D. B. F., 2007b. Articular damage caused by metal plugs in a rabbit model for treatment of localized cartilage defects. Osteoarthritis and Cartilage 15 (8), 937–945.

Custers, R. J. H., Saris, D. B. F., Creemers, L. B., Verbout, A. J., van Rijen, M. H. P., Mastbergen, S. C., Lafeber, F. P., Dhert, W. J. A., 2010b. Replacement of the medial tibial plateau by a metallic implant in a goat model. Journal of Orthopaedic Research 28 (4).

Custers, R. J. H., Saris, D. B. F., Dhert, W. J. A., Verbout, A. J., van Rijen, M. H. P., Mastbergen, S. C., Lafeber, F. P. J. G., Creemers, L. B., 2009b. Articular cartilage degeneration following the treatment of focal cartilage defects with ceramic metal implants and compared with microfracture. Journal of Bone and Joint Surgery - Series A 91 (4), 900–910.

Davy, D. T., Kotzar, G. M., Brown, R. H., Heiple, K. G., Goldberg, V. M., Heiple Jr., K. G., Berilla, J., Burstein, A. H., 1988. Telemetric force measurements across the hip after total arthroplasty. Journal of Bone and Joint Surgery - Series A 70 (1), 45–50.

DiSilvestro, M. R., Suh, J.-K. F., 2001. A cross-validation of the biphasic poroviscoelastic model of articular cartilage in unconfined compression, indentation, and confined compression. Journal of Biomechanics 34 (4), 519–525.

DiSilvestro, M. R., Zhu, Q., Suh, J.-K. F., 2001a. Biphasic poroviscoelastic simulation of the unconfined compression of articular cartilage: Ii - effect of variable strain rates. Journal of Biomechanical Engineering 123 (2), 198–200.

DiSilvestro, M. R., Zhu, Q., Wong, M., Jurvelin, J. S., Suh, J.-K. F., 2001b. Biphasic poroviscoelastic simulation of the unconfined compression of articular cartilage: I - simultaneous prediction of reaction force and lateral displacement. Journal of Biomechanical Engineering 123 (2), 191–197.

D'Lima, D. D., Patil, S., Steklov, N., Chien, S., Colwell Jr., C. W., 2007. In vivo knee moments and shear after total knee arthroplasty. Journal of Biomechanics 40 (SUPPL. 1), S11–S17.

D'Lima, D. D., Patil, S., Steklov, N., Slamin, J. E., Colwell Jr., C. W., 2006. Tibial forces measured in vivo after total knee arthroplasty. Journal of Arthroplasty 21 (2), 255–262.

D'Lima, D. D., Steklov, N., Fregly, B. J., Banks, S. A., Colwell Jr., C. W., 2008a. In vivo contact stresses during activities of daily living after knee arthroplasty. Journal of Orthopaedic Research 26 (12), 1549–1555.

D'Lima, D. D., Steklov, N., Patil, S., Colwell Jr., C. W., 2008b. The mark coventry award: In vivo knee forces during recreation and exercise after knee arthroplasty. Clinical Orthopaedics and Related Research 466 (11), 2605–2611.

D'Lima, D. D., Townsend, C. P., Arms, S. W., Morris, B. A., Colwell Jr., C. W., 2005. An implantable telemetry device to measure intra-articular tibial forces. Journal of Biomechanics 38 (2), 299–304.

Donzelli, P. S., Spilker, R. L., Ateshian, G. A., Mow, V. C., 1999. Contact analysis of biphasic transversely isotropic cartilage layers and correlations with tissue failure. Journal of Biomechanics 32 (10), 1037–1047.

Duda, G. N., Maldonado, Z. M., Klein, P., Heller, M. O. W., Burns, J., Bail, H., 2005. On the influence of mechanical conditions in osteochondral defect healing. Journal of Biomechanics 38 (4), 843–851.

Federico, S., Herzog, W., 2008. On the anisotropy and inhomogeneity of permeability in articular cartilage. Biomechanics and Modeling in Mechanobiology 7 (5), 367–378.

Fukubayashi, T., Kurosawa, H., 1980. The contact area and pressure distribution pattern of the knee. a study of normal and osteoarthrotic knee joints. Acta Orthopaedica Scandinavica 51 (6), 871–879.

Garcia, J. J., Altiero, N. J., Haut, R. C., 1998. An approach for the stress analysis of transversely isotropic biphasic cartilage under impact load. Journal of Biomechanical Engineering 120 (5), 608–613.

Gerber, B. E., Robinson, D., Nevo, Z., Brosh, T., Ash, H., Yayon, A., Aviezer, D., 2002. Mechanical resistance of biological repair cartilage: Comparative in vivo tests of different surgical repair procedures. International Journal of Artificial Organs 25 (11), 1109–1115.

Getgood, A., Bhullar, T. P. S., Rushton, N., 2009. Current concepts in articular cartilage repair. Orthopaedics and Trauma 23 (3), 189–200.

Guettler, J. H., Demetropoulos, C. K., Yang, K. H., Jurist, K. A., 2004. Osteochondral defects in the human knee: Influence of defect size on cartilage rim stress and load redistribution to surrounding cartilage. American Journal of Sports Medicine 32 (6), 1451–1458.

Hangody, L., Feczkó, P., Bartha, L., Bodó, G., Kish, G., 2001. Mosaicplasty for the treatment of articular defects of the knee and ankle. Clinical orthopaedics and related research (391 SUPPL.).

Hangody, L., Füles, P., 2003. Autologous osteochondral mosaicplasty for the treatment of full-thickness defects of weight-bearing joints: Ten years of experimental and clinical experience. Journal of Bone and Joint Surgery - Series A 85 (SUPPL. 1), 25–32.

Hayes, W. C., Keer, L. M., Herrmann, G., Mockros, L. F., 1972. A mathematical analysis for indentation tests of articular cartilage. Journal of Biomechanics 5 (5), 541–551.

Heinlein, B., Graichen, F., Bender, A., Rohlmann, A., Bergmann, G., 2007. Design,calibration and pre-clinical testing of an instrumented tibial tray. Journal of Biomechanics 40 (SUPPL. 1), S4–S10.

Heinlein, B., Kutzner, I., Graichen, F., Bender, A., Rohlmann, A., Halder, A. M., Beier, A., Bergmann, G., 2009. Esb clinical biomechanics award 2008: Complete data of total knee replacement loading for level walking and stair climbing measured in vivo with a follow-up of 6-10 months. Clinical Biomechanics 24 (4), 315–326.

HemiCAP^{TM}, 2002. made by arthrosurface,http://www. arthrosurface. com/.

Hibbitt, Karlson, Sorenson, 2007. ABAQUS Version 6. 7: Theory manual,User's manual,Verification manual and Example problems manual.

Hjelle, K., Solheim, E., Strand, T., Muri, R., Brittberg, M., 2002. Articular cartilage defects in 1,000 knee arthroscopies. Arthroscopy 18 (7), 730–734.

Hosseini, A., Van de Velde, S. K., Kozanek, M., Gill, T. J., Grodzinsky, A. J., Rubash, H. E., Li, G., 2010. In-vivo time-dependent articular cartilage contact behavior of the tibiofemoral joint. Osteoarthritis and Cartilage 18 (7), 909–916.

Julkunen, P., Kiviranta, P., Wilson, W., Jurvelin, J. S., Korhonen, R. K., 2007. Characterization of articular cartilage by combining microscopic analysis with a fibril-reinforced finite-element model. Journal of Biomechanics 40 (8), 1862–1870.

Jurvelin, J. S., Buschmann, M. D., Hunziker, E. B., 2003. Mechanical anisotropy of the human knee articular cartilage in compression. Proceedings of the Institution of Mechanical Engineers,Part H: Journal of Engineering in Medicine 217 (3), 215–219.

Kaufman, K. R., Kovacevic, N., Irby, S. E., Colwell, C. W., 1996. Instrumented implant for measuring tibiofemoral forces. Journal of Biomechanics 29 (5), 667–671.

Kempson, G. E., Freeman, M. A. R., Swanson, S. A. V., 1971. The determination of a creep modulus for articular cartilage from indentation tests on the human femoral head. Journal of Biomechanics 4 (4), 239–250.

Kirker-Head, C. A., van Sickle, D. C., Ek, S. W., McCool, J. C., 2006. Safety of,and biological and functional response to,a novel metallic implant for the management of focal full-thickness cartilage defects: Preliminary assessment in an animal model out to 1 year. Journal of Orthopaedic Research 24 (5), 1095–1108.

Kirking, B., Krevolin, J., Townsend, C., Colwell Jr., C. W., D'Lima, D. D., 2006. A multiaxial force-sensing implantable tibial prosthesis. Journal of Biomechanics 39 (9), 1744–1751.

Komistek, R. D., Dennis, D. A., Mabe, J. A., 1998. In-vivo determination of patellofemoral separation and linear impulse forces [die in-vivo-bestimmung der patellofemoralen entkopplung und der linearen impulskrafte]. Orthopade 27 (9), 612–618.

Komistek, R. D., Dennis, D. A., Mahfouz, M., 2003. In vivo fluoroscopic analysis of the normal human knee. Clinical Orthopaedics and Related Research (410), 69–81.

Komistek, R. D., Kane, T. R., Mahfouz, M., Ochoa, J. A., Dennis, D. A., 2005. Knee mechanics: A review of past and present techniques to determine in vivo loads. Journal of Biomechanics 38 (2), 215–228.

Komistek, R. D., Stiehl, J. B., Dennis, D. A., Paxson, R. D., Soutas-Little, R. W., 1997. Mathematical model of the lower extremity joint reaction forces using kane's method of dynamics. Journal of Biomechanics 31 (2), 185–189.

Kuster, M. S., Wood, G. A., Stachowiak, G. W., Gächter, A., 1997. Joint load considerations in total knee replacement. Journal of Bone and Joint Surgery - Series B 79 (1), 109–113.

Kutzner, I., Heinlein, B., Graichen, F., Bender, A., Rohlmann, A., Halder, A., Beier, A., Bergmann, G., 2010. Loading of the knee joint during activities of daily living measured in vivo in five subjects. Journal of Biomechanics 43 (11), 2164–2173.

Lai, W. M., Hou, J. S., Mow, V. C., 1991. A triphasic theory for the swelling and deformation behaviors of articular cartilage. Journal of Biomechanical Engineering 113 (3), 245–258.

Lai, W. M., Mow, V. C., 1980. Drag-induced compression of articular cartilage during a permeation experiment. Biorheology 17 (1-2), 111–123.

Lai, W. M., Mow, V. C., Roth, V., 1981. Effects of nonlinear strain-dependent permeability and rate of compression on the stress behavior of articular cartilage. Journal of Biomechanical Engineering 103 (2), 61–66.

Lai, W. M., Mow, V. C., Zhu, W., 1993. Constitutive modeling of articular cartilage and biomacromolecular solutions. Journal of Biomechanical Engineering 115 (4 B), 474–480.

Lefkoe, T. P., Trafton, P. G., Ehrlich, M. G., Walsh, W. R., Dennehy, D. T., Barrach, H. J., Akelman, E., 1993. An experimental model of femoral condylar defect leading to osteoarthrosis. Journal of orthopaedic trauma 7 (5), 458–467.

Li, L. P., Buschmann, M. D., Shirazi-Adl, A., 2000. A fibril reinforced nonhomogeneous poroelastic model for articular cartilage: Inhomogeneous response in unconfined compression. Journal of Biomechanics 33 (12), 1533–1541.

Manda, K., Ryd, L., Eriksson, A., 2010. Finite element simulations of a focal knee resurfacing implant applied to localized cartilage defects in a sheep model. Journal of Biomechanics (submitted).

Mansour, J. M., Mow, V. C., 1976. The permeability of articular cartilage under compressive strain and at high pressures. Journal of Bone and Joint Surgery - Series A 58 (4), 509–516.

Martini, L., Fini, M., Giavaresi, G., Giardino, R., 2001. Sheep model in orthopedic research: A literature review. Comparative medicine 51 (4), 292–299.

Mittra, E., Rubin, C., Qin, Y. ., 2005. Interrelationship of trabecular mechanical and microstructural properties in sheep trabecular bone. Journal of Biomechanics 38 (6), 1229–1237.

Morrison, J. B., 1970. The mechanics of the knee joint in relation to normal walking. Journal of Biomechanics 3 (1), 51–61.

Mow, V. C., Ateshian, G. A., Spiiker, R. L., 1993. Biomechanics of diarthrodial joints: A review of twenty years of progress. Journal of Biomechanical Engineering 115 (4 B), 460–467.

Mow, V. C., Gu, W. Y., Chen, F. H., 2004. Structure and function of articular cartilage and meniscus. Basic Orthopaedic Biomechanics and Mechano-Biology, Lippincott Williams and Wilkins, 3rd edition, 181–258.

Mow, V. C., Hung, C. T., 2001. Biomechanics of articular cartilage. Basic Biomechanics of the Musculoskeletal System, Editors: Nordin, M. and Frankel, V. H. , 3rd ed. Philadelphia, PA, USA: Lippincott Williams and Wilkins, 60–100.

Mow, V. C., Kuei, S. C., Lai, W. M., Armstrong, C. G., 1980. Biphasic creep and stress relaxation of articular cartilage in compression: Theory and experiments. Journal of Biomechanical Engineering 102 (1), 73–84.

Mündermann, A., Dyrby, C. O., D'Lima, D. D., Colwell Jr., C. W., Andriacchi, T. P., 2008. In vivo knee loading characteristics during activities of daily living as measured by an instrumented total knee replacement. Journal of Orthopaedic Research 26 (9), 1167–1172.

O'Driscoll, S. W., 1998. The healing and regeneration of articular cartilage. Journal of Bone and Joint Surgery - Series A 80 (12), 1795–1812.

Oloyede, A., Broom, N. D., 1991. Is classical consolidation theory applicable to articular cartilage deformation? Clinical Biomechanics 6 (4), 206–212.

Paul, J. P., 1976. Approaches to design. force actions transmitted by joints in the human body. Proceedings of the Royal Society of London - Biological Sciences 192 (1107), 163–172.

Pawaskar, S. S., Jin, Z. M., Fisher, J., 2007. Modelling of fluid support inside articular cartilage during sliding. Proceedings of the Institution of Mechanical Engineers,Part J: Journal of Engineering Tribology 221 (3), 165–174.

Peña, E., Calvo, B., Martínez, M. A., Doblaré, M., 2007. Effect of the size and location of osteochondral defects in degenerative arthritis. A finite element simulation. Computers in Biology and Medicine 37 (3), 376–387.

Radin, E. L., Orr, R. B., Kelman, J. L., 1982. Effect of prolonged walking on concrete on the knees of sheep. Journal of Biomechanics 15 (7), 487–492.

Reynaud, B., Quinn, T. M., 2006. Anisotropic hydraulic permeability in compressed articular cartilage. Journal of Biomechanics 39 (1), 131–137.

Seireg, A., Arvikar, R. J., 1973. A mathematical model for evaluation of forces in lower extremeties of the musculo skeletal system. Journal of Biomechanics 6 (3), 313–326.

Seireg, A., Arvikar, R. J., 1975. The prediction of muscular load sharing and joint forces in the lower extremities during walking. Journal of Biomechanics 8 (2), 89–102.

Simon, B. R., 1992. Multiphase poroelastic finite element models for soft tissue structures. Applied Mechanics Reviews 45 (6), 191–218.

Simon, T. M., Jackson, D. W., 2006. Articular cartilage: Injury pathways and treatment options. Sports Medicine and Arthroscopy Review 14 (3), 146–154.

Smith, C. L., Mansour, J. M., 2000. Indentation of an osteochondral repair: Sensitivity to experimental variables and boundary conditions. Journal of Biomechanics 33 (11), 1507–1511.

Soltz, M. A., Ateshian, G. A., 2000. A conewise linear elasticity mixture model for the analysis of tension-compression nonlinearity in articular cartilage. Journal of Biomechanical Engineering 122 (6), 576–586.

Song, Y., Greve, J. M., Carter, D. R., Giori, N. J., 2008. Meniscectomy alters the dynamic deformational behavior and cumulative strain of tibial articular cartilage in knee joints subjected to cyclic loads. Osteoarthritis and Cartilage 16 (12), 1545–1554.

Song, Y., Greve, J. M., Carter, D. R., Koo, S., Giori, N. J., 2006. Articular cartilage MR imaging and thickness mapping of a loaded knee joint before and after meniscectomy. Osteoarthritis and Cartilage 14 (8), 728–737.

Soulhat, J., Buschmann, M. D., Shirazi-Adl, A., 1999. A fibril-network-reinforced biphasic model of cartilage in unconfined compression. Journal of Biomechanical Engineering 121 (3), 340–347.

Suh, J. K., Bai, S., 1998. Finite element formulation of biphasic poroviscoelastic model for articular cartilage. Journal of Biomechanical Engineering 120 (2), 195–201.

Taylor, S. J. G., Gorjon, J., Walker, P. S., 1999. An instrumented prosthesis for knee joint force measurement in vivo. IEE Colloquium (Digest) (89), 25–28.

Taylor, S. J. G., Perry, J. S., Meswania, J. M., Donaldson, N., Walker, P. S., Cannon, S. R., 1997. Telemetry of forces from proximal femoral replacements and relevance to fixation. Journal of Biomechanics 30 (3), 225–234.

Taylor, S. J. G., Walker, P. S., 2001. Forces and moments telemetered from two distal femoral replacements during various activities. Journal of Biomechanics 34 (7), 839–848.

Taylor, S. J. G., Walker, P. S., Perry, J. S., Cannon, S. R., Woledge, R., 1998. The forces in the distal femur and the knee during walking and other activities measured by telemetry. Journal of Arthroplasty 13 (4), 428–435.

Taylor, W. R., Ehrig, R. M., Heller, M. O., Schell, H., Seebeck, P., Duda, G. N., 2006. Tibio-femoral joint contact forces in sheep. Journal of Biomechanics 39 (5), 791–798.

Taylor, W. R., Heller, M. O., Bergmann, G., Duda, G. N., 2004. Tibio-femoral loading during human gait and stair climbing. Journal of Orthopaedic Research 22 (3), 625–632.

Temenoff, J. S., Mikos, A. G., 2000. Review: Tissue engineering for regeneration of articular cartilage. Biomaterials 21 (5), 431–440.

Thambyah, A., Pereira, B. P., Wyss, U., 2005. Estimation of bone-on-bone contact forces in the tibiofemoral joint during walking. Knee 12 (5), 383–388.

van der Voet, A., 1997. A comparison of finite element codes for the solution of biphasic poroelastic problems. Proceedings of the Institution of Mechanical Engineers. Part H,Journal of engineering in medicine 211 (2), 209–211.

Varadarajan, K. M., Moynihan, A. L., D'Lima, D., Colwell, C. W., Li, G., 2008. In vivo contact kinematics and contact forces of the knee after total knee arthroplasty during dynamic weight-bearing activities. Journal of Biomechanics 41 (10), 2159–2168.

Vaziri, A., Nayeb-Hashemi, H., Singh, A., Tafti, B. A., 2008. Influence of meniscectomy and meniscus replacement on the stress distribution in human knee joint. Annals of Biomedical Engineering 36 (8), 1335–1344.

Walker, P. S., Erkman, M. J., 1975. The role of the menisci in force transmission across the knee. Clinical Orthopaedics No. 109, 184–192.

Wang, C. C. ., Hung, C. T., Mow, V. C., 2001. An analysis of the effects of depth-dependent aggregate modulus on articular cartilage stress-relaxation behavior in compression. Journal of Biomechanics 34 (1), 75–84.

Wilson, W., Van Donkelaar, C. C., Van Rietbergen, B., Huiskes, R., 2005a. A fibril-reinforced poroviscoelastic swelling model for articular cartilage. Journal of Biomechanics 38 (6), 1195–1204.

Wilson, W., Van Donkelaar, C. C., Van Rietbergen, B., Ito, K., Huiskes, R., 2004. Stresses in the local collagen network of articular cartilage: A poroviscoelastic fibril-reinforced finite element study. Journal of Biomechanics 37 (3), 357–366.

Wilson, W., Van Donkelaar, C. C., Van Rietbergen, R., Huiskes, R., 2005b. The role of computational models in the search for the mechanical behavior and damage mechanisms of articular cartilage. Medical Engineering and Physics 27 (10), 810–826.

Wilson, W., van Rietbergen, B., van Donkelaar, C. C., Huiskes, R., 2003. Pathways of load-induced cartilage damage causing cartilage degeneration in the knee after meniscectomy. Journal of Biomechanics 36 (6), 845–851.

Wimmer, M. A., Andriacchi, T. P., 1997. Tractive forces during rolling motion of the knee: Implications for wear in total knee replacement. Journal of Biomechanics 30 (2), 131–137.

Wu, J. Z., Herzog, W., Epstein, M., 1997. Evaluation of the finite element software ABAQUS for biomechanical modelling of biphasic tissues. Journal of Biomechanics 31 (2), 165 – 169.

Xia, Y., Ramakrishnan, N., Bidthanapally, A., 2007. The depth-dependent anisotropy of articular cartilage by fourier-transform infrared imaging (FTIRI). Osteoarthritis and Cartilage 15 (7), 780–788.

Zarrinkalam, M. R., Beard, H., Schultz, C. G., Moore, R. J., 2009. Validation of the sheep as a large animal model for the study of vertebral osteoporosis. European Spine Journal 18 (2), 244–253.

Zhao, D., Banks, S. A., D'Lima, D. D., Colwell Jr., C. W., Fregly, B. J., 2007. In vivo medial and lateral tibial loads during dynamic and high flexion activities. Journal of Orthopaedic Research 25 (5), 593–602.